All-in-one AAV-delivered epigenome-editing platform: *proof-of-concept* and therapeutic implications for neurodegenerative disorders

Boris Kantor[1,2,3,]†, Bernadette Odonovan[4,5,]*, Joseph Rittiner[1,2,3,]*, Nicholas Lindner[1,2,3], Wendy Dong[1,2,3], Austin Zhang[1,2,3], Peter Nicholls[4,5], Ornit Chiba-Falek[4,5,]†

[1]Department of Neurobiology, [2]Viral Vector Core, [3]Center for Advanced Genomic Technologies, [4]Division of Translational Brain Sciences, Department of Neurology, [5]Center for Genomic and Computational Biology, Duke University School of Medicine, Durham, NC 27710, USA

* These authors equally contributed to the manuscript
† To whom correspondence should be addressed:

Ornit Chiba-Falek
Division of Translational Brain Sciences, Department of Neurology
Duke University School of Medicine
Durham, North Carolina 27710, USA
Phone: 919-681-8001
Fax: 919-613-6448
Email: o.chibafalek@duke.edu

Boris Kantor
Department of Neurobiology
Duke University School of Medicine
Durham, North Carolina 27707, USA
Phone: 919-681-1068
Email: boris.kantor@duke.edu

Keywords: Adeno-Associated Vector (AAV); Clustered regularly-interspaced short palindromic repeats / CRISPR-associated protein 9 (CRISPR/Cas9); transcriptional repressor, epigenome-based editing; all-in-one delivery system; *APOE*; Alzheimer's disease (AD).
Number of Figures: 4
Number of Tables: 0

Abstract

Safely and efficiently controlling gene expression is a long-standing goal of biomedical research, and the recently discovered bacterial CRISPR/Cas system can be harnessed to create powerful tools for epigenetic editing. Current state-of-the-art systems consist of a deactivated-Cas9 nuclease (dCas9) fused to epigenetic effector motifs/domains, along with a guide RNA (gRNA) which defines the genomic target. Such systems have been used to safely and effectively silence or activate a specific gene target under a variety of circumstances. Adeno-associated virus (AAV) vectors are the therapeutic platform of choice for delivery of genetic cargoes; nevertheless, their small packaging capacity is not suitable for the delivery of large constructs, including most CRISPR/dCas9-effector systems. To circumvent this, many AAV-based CRISPR/Cas tools are delivered separately from two viral cassettes. However, this approach requires higher viral payloads and usually is less efficient. Here we develop a compact dCas9-based repressor system packaged within a single, optimized AAV vector. The system uses a smaller dCas9 variant derived from *Staphylococcus aureus* (*Sa*). A novel repressor was engineered by fusing the small transcription repression domain (TRD) from MeCP2 with the KRAB repression domain. The final d*Sa*Cas9-KRAB-MeCP2(TRD) construct can be efficiently packaged, along with its associated gRNA, into AAV particles. Using reporter assays, we demonstrate that the platform is capable of robustly and sustainably repressing the expression of multiple genes-of-interest, both *in vitro* and *in vivo*. Most relevantly, we successfully silenced *APOE*, the primary genetic risk factor for late onset Alzheimer's disease (LOAD). This new platform will broaden the CRISPR/dCas9 toolset available for transcriptional manipulation of gene expression in research and therapeutic settings.

Introduction

Bacterial Clustered Regularly Interspaced Palindromic Repeats (CRISPR)/Cas systems have evolved to bind and cleave nucleic acids in a highly-efficient and flexible fashion [1], [2], [3]. Since their discovery, various Cas orthologs and variants with useful properties have been identified and harnessed for use in gene editing. Unfortunately, gene-editing approaches employing active, wild-type Cas9 endonucleases have resulted in unwanted off-target effects, including cell cycle arrest, changes in cellular differentiation, and apoptotic signaling, which are serious barriers against the use of this technology in gene therapy applications [4], [5], [6]. Earlier studies have shown that point mutations introduced into the catalytic domains of Cas9 enzymes can completely abolish their endonuclease activity without affecting their affinity for the targeted DNA [7], [8], [9], [10]. Furthermore, by fusing epigenetic effectors or domains with the catalytically-inactive, or 'dead', Cas9 (dCas9), the expression of target genes can be increased or decreased through epigenetic editing [9], [11], [12], [13], [14]. This approach (repurposing the CRISPR/Cas system for gene activation or repression) has been coined CRISPR-activation (CRISPRa) or CRISPR-interference (CRISPRi), respectively. A variety of these tools, including those based on DNA methyltransferases (DNMTs), transcriptional repressors, and histone-modifying enzymes (HMEs) have been developed, with many achieving strong levels of gene repression (reviewed in [15]). These approaches are also applicable in a clinical setting, and targeted regulation of disease-causal genes offers novel avenues for the development of a new generation of gene therapies [16], [17], [18]. For example, our laboratory recently developed an all-in-one lentiviral vector expressing dCas9 fused to the catalytic domain of DNA methyltransferase 3A (DNMT3A) for targeted repression of the *SNCA* gene, as a therapeutic strategy for Parkinson's Disease (PD) [19, 20]. We showed that the reduction in *SNCA* levels mediated by the [*SNCA* gRNA]/dCas9-DMNT3A system successfully rescued disease-related cellular phenotypes including the production of mitochondrial reactive oxygen species (ROS) and cellular viability of dopaminergic neurons [19], [20].

As with many other gene therapy tools, CRISPR/Cas components are commonly delivered *via* viral vectors (reviewed in [15]). Lentiviral vectors (LVs) and adeno-associated vectors (AAVs) offer an effective way for gene-to-cell transfer, and as such these platforms occupy a central place among delivery systems used for gene therapy applications. LVs are attractive delivery vehicles due to their ability to accommodate large transgenic payloads and sustain a robust level of gene expression in a wide range of dividing and non-dividing cells (reviewed in [21]). However, long-term expression of LV-delivered Cas9/guide RNA systems may lead to substantial undesirable off-target perturbations characterized by non-specific RNA-DNA interactions and off-target DNA cleavage [22]. Furthermore, as an integrating system, LVs possess a significant risk of insertional mutagenicity, and even oncogenicity [23]. Recombinant AAV vectors, on the other hand, offer a transiently expressing platform, along with very weak integration capacity. Recent advances in the development of preclinically and clinically graded AAVs have propelled this system into broad use in the gene therapy field. Indeed, preclinical and therapeutic successes in AAV-based gene replacement and gene editing have helped AAV to gain a reputation as a leading therapeutic platform, with two AAV-mediated gene therapy products recently gaining regulatory approval in Europe and the United States (reviewed in [24]).

However, a major limitation of using AAV vectors is their relatively small transgene capacity (up to approximately 4.6kb), which makes it difficult (or outright impossible) to package bulky transgenes. For instance, the coding sequence of *Streptococcus pyogenes* Cas9 (SpCas9) is 4.2kb, which consumes essentially nearly all of the packaging room of the vector. The discovery of smaller Cas9 enzymes, including those derived from *Staphylococcus aureus* (SaCas9), *Campylobacter jejuni* (CjCas9),

Deltaproteobacteria (CasX), and most recently a miniature Cas system (CasMINI) engineered from the type V-F Cas12f (Cas14), has led to the development of Cas/guide RNA systems which are more suitable to be packaged into AAV vectors [25], [26], [27], [28]. Furthermore, all the above endonucleases have been successfully converted into their respective non-active versions to support various gene-repurposing applications. For example, Thakore and colleagues developed a dSaCas9-KRAB repressor system packaged in AAV particles [29]. Nevertheless, the authors utilized a dual-AAV system, delivering dSaCas9-KRAB and a *PCSK9*-targeting gRNA from two separate expression cassettes to repress the transcription of PCSK9 (a regulator of cholesterol levels) in the liver of adult mice [29].

The value of an improved Cas-effector pairing would be immense, considering that in addition to the CRISPR/Cas components the vector has to accommodate at least two promoters (a traditional Pol II promoter to express the Cas9-repressor protein, and a Pol III promoter to express the gRNA component), a poly(A) signal for transcriptional termination, and nuclear localization signals (NLSs), as well as other *cis-acting* elements such as Woodchuck hepatitis virus Posttranscriptional Regulatory Element (WPRE).

Furthermore, AAV-based systems are significantly more sensitive than other vectors (*e.g.* LVs) when it comes to packaging of multipart components, such as CRISPR/Cas [24]. As a consequence, most of the all-in-one CRISPR/Cas9 tools developed so far are based on plasmid-based or lentiviral delivery systems [30], [31]. [32], [33]. We recently demonstrated that the tolerability of the vector systems towards accommodation of sophisticated gene-editing tools, their packaging efficiency and viral titers could be significantly improved by the optimizations made within the vector backbone. Using integrase-deficient (IDLV) and integrase-competent (ICLV) lentiviral vectors, we demonstrated that IDLV-CRISPR/Cas and ICLV-CRISPR/Cas constructs carrying multiple binding sites for the transcription factors Sp1 and NF-kB could be packaged more efficiently and produced at higher titers [22]. Furthermore, functional titers (measured at the transduced cells) also showed a significant improvement compared to the naïve viral counterparts [22]. The improved vectors were able to mediate efficient and robust gene editing perturbations *in vitro* and *in vivo.* Lastly, the IDLV-CRISPR/Cas vector showed only minimal off-target effects, and majority of its genome remains in an episomal (non-integrated) state.

Notably, most recombinant vectors, including LVs and AAVs, are lacking many of their endogenous elements, including the above Sp1 and NF-kB sites, which are deleted from vector cassettes along with larger elements, primarily due to safety reasons [19], [22], [34]. Thus, most episomal vectors, including IDLV, AAV, Cytomegalovirus (CMV), Epstein-Barr virus (EBV) and Herpes simplex virus type 1 (HSV-1) inherit the limitation of being epigenetically silenced by default. We and other research groups have studied the early stages of the viral life cycle and reported a competition between cellular epigenetic silencing of viral genes and viral inhibition of repressive factors, such as virus-encoded histone deacetylases (HDACs) and other factors [22] [35], [36], [37], [38]. Therefore, a lack of activation machinery utilizing these transcriptional factors could distort the transcriptional environment on the chromatin level, resulting in transcriptional silencing and general impairment of viral expression [22] [39]. AAV is a prominent example as its genome is organized into repressive, silencing chromatin structures [21], [22]. Furthermore, the expression cassettes of rAAVs are scrubbed of Sp1 and NF-kB binding sites [40], [41], [42]. Here, we developed and validated an improved AAV vector carrying a concatemer of the Sp1 & NF-kB recognition sites in its expression cassette. We then used the optimized vector backbone to screen for epigenetic editors efficiently packaged into all-in-one AAV particles. The lead platform harbored dSaCas9 fused to transcriptional repression domains (TRDs) domains derived from MeCP2 and KRAB. The system could be efficiently packaged into AAV, and robustly suppressed gene expression *in*

vitro and *in vivo*. This novel platform can expand the AAV/CRISPR-dCas9 toolbox for both basic research and preclinical/clinical studies.

Results

Optimization of AAV vector backbone

The genome of recombinant AAV harbors no Sp1 and NF-kB binding sites, unlike the wild type virus [19], [22], [34], [40], [41], [42]. As a first step to build an efficient epigenome-editing system for AAV delivery, we decided to reintroduce the above transcription activator binding sites into the expression cassette of the vector. We inserted 2xSp1, 4xSp1, 2xNF-kB, 4xNF-kB, and 2xSp1+2xNF-kB binding sites into the backbone of an AAV vector expressing a dual dGFP/NanoLuc reporter **(Fig. 1a).** All sites were cloned upstream from the core (minimal) portion of the EF1α promoter, dubbed EFS-NC. The naïve EFS-NC promoter (which carries neither Sp1 nor NF-kB binding sites) was used as a control. In addition, a full-length version of the EF1α promoter, which contains multiple Sp1 and NF-kB sites was used as a positive control. The full-length EF1α promoter is ubiquitous and strong, but its large size (~1500bps) generally is not suitable for AAV packaging. However, the miniature EFS-NC promoter (only 212 bps long) fits most transgenes expressed via AAV systems. To test whether the above modifications would improve the packaging efficiency and transcription, the vectors were first manufactured at non-concentrated grades and titered by real-time PCR**.** We did not observe any significant differences between the titered vectors **(Fig. 1b)**, suggesting that the above modifications did not affect the physical AAV packaging process. Next, titer-normalized vectors were transduced into HEK293T cells at MOI=10,000. As shown in **Fig. 1c**, expression from vectors harboring Sp1 and NF-kB sites was higher than that of the naïve EFS-NC counterpart. Furthermore, the vectors carrying four repeats showed higher levels of nLuc expression compared to those with two repeats (**Fig. 1c).** The observed increase was close to 4-fold in the samples with 4 Sp1 or 4 NF-kB, and slightly higher increase in the sample bearing 2xSp1+2xNF-kB. Indeed, expression from the latter vector was only slightly lower than that shown by the vector carrying a complete copy of the EF1α promoter (**Fig. 1c).** This suggests that most of the enhancer activity provided by the distal (non-core) portions of the EF1α promoter is supplied by the binding of transcription factors Sp1 and NF-kB. The restoration of their binding sites within the expression plasmid had a major impact on the expression of the reporter transgene delivered by the viral vector.

All-in-one AAV gene repression platform

Next, we engineered a gene-silencing platform that fits within AAV size restrictions. We utilized a screening strategy based on a dual reporter system, outlined in **Fig 2a**. A reporter vector expressing destabilized GFP (dGFP) and NanoLuciferase (nLuc) genes was packaged into LV particles. The expression vector cassette also carried a puromycin resistance marker for selection. We then used HEK293T cells to create a stable reporter cell line. The cells were transduced at MOI=0.2 to ensure integration at the rate of 1 copy per cell. The dGFP and nLuc proteins were expressed from the CMV promoter, which was targeted with appropriate gRNAs (**Fig. 2a & 2f).** Two gRNAs sequences were selected to target the reporter construct (**Fig. 2f**; gRNA1 and gRNA2). Importantly, both dGFP and nLuc are characterized by short protein half-lives, making them ideal for the evaluation of gene expression changes. In this study we focused on the catalytically inactive mutants of two small Cas9 proteins, derived from *Campylobacter jejuni* (dCjCas9) and *Staphylococcus aureus* (dSaCas9) (**Fig. 2a & 2f)**.

These proteins were then fused with a panel of repressors for the screening: First, dCjCas9 and dSaCas9 were fused with heterochromatin proteins 1a and 1b (HP1a and HP1b, respectively) **(**[44] and **Fig. 2b)**. Here, we decided to use the repressive chromoshadow domain (CSD) of HP1 both with and without the hinge region. The chromoshadow domain is responsible for the multimerization of HP1 and the formation/maintenance of compact heterochromatin structures, while the hinge region is responsible

for additional transcriptional regulation via interaction with histone H3 and other repressive effectors **(**[37], [45], and **Fig. 2b).** Secondly, we investigated TRDs from the methyl-CpG-binding domain (MBD) protein family **(Fig. 2c)**. This family contains Methyl-CpG-binding domain proteins 1, 2, and 3 (MBD1-3 respectively), and methyl CpG binding protein 2 (MeCP2) **(Fig. 2c)**. The MBD1-3 and MeCP2 TRDs are responsible for the repression mediated by these proteins [43]. As mentioned above, we previously developed a lentivirus carrying a dCas9-DNMT3A transgene for epigenome editing of the Parkinson's risk-factor gene *SNCA* [19], [20], [46]. As such, a third group of repressors was also used in this study, based on DNA methyltransferases 3A and 3B (DNMT3A and DNMT3B) (**Fig. 2d)**. Lastly, we included a few miscellaneous repression domains: the TRD from Nuclear inhibitor of protein phosphatase 1 (NIPP1), a representative Krüppel associated box (KRAB) domain from Zinc finger protein 10 (KOX1), and a novel KRAB-MeCP2(TRD) combination (**Fig. 2e)**.

The corresponding plasmids were packaged into AAV2/9 viral particles and concentrated as described in Materials and Methods, and the titers of the produced vectors were measured by real-time PCR. All vectors, except those carrying DNMT3A or DNMT3B, consistently achieved very high physical titers **(Fig. 3a, b)**. This was not unexpected. The sizes of this family of vectors were largely either within or slightly over the nominal AAV packaging capacity of 4.6kb (see Materials and Methods). However, as other groups have found, even slightly oversized genomes can be efficiently packaged within an optimized AAV vector cassette; however, extremely bulky vectors such as dCjCas9-DNMT3A/B (~5.1kb) and dSaCas9-DNMT3A/B (~5.4kb) could not be efficiently packaged even into the optimized AAV, resulting in dramatically lower titers **(Fig. 3a, b)**. Notably, the physical titers obtained from the rest of the vectors produced here were similar to those obtained from a naïve vector carrying no CRISPR/Cas components **(**[23] and **Fig. 3a, b)**.

Next, the vectors were titer-normalized and transduced into the HEK293T reporter cell line (see Fig. 2a) to evaluate their repressive effects. The cells were harvested at day 4 post transduction, total protein was normalized via BCA assay, and a luciferase assay was performed. Importantly, no detectable reduction in nLuc expression was reported in any of the samples transduced with vectors not expressing a CMV-targeting gRNA (across all effectors, plus a no-gRNA/no-effector control), compared to naive control cells **(Fig. 3c, d)**. However, most samples transduced with vectors expressing dCj/SaCas-effector + [CMV gRNA] showed reduced nLuc expression (**Fig. 3c, d)**. The main exception to this was the MBD3 containing vectors, none of which resulted in a measurable reduction of nLuc (**Fig. 3c, d)**. Zooming in on the repression capacity of the selected effectors: HP1a and HP1b constructs containing the hinge in addition to the CSD performed slightly better than their CSD-only counterparts (**Fig. 3c, d)**. MBD1-, MBD2-, and NIPP1-containg constructs showed moderate levels of repression, but generally less than the HP1 family (**Fig. 3c, d)**. As mentioned above, MBD3 was completely inactive. Finally, while the dCj/SaCas9-KRAB and dCj/SaCas9-MeCP2(TRD) constructs each individually resulted in significant levels of repression, their combination, dCj/SaCas9-KRAB-MeCP2(TRD), clearly demonstrated the most substantial silencing observed in the entire screen by a substantial margin (**Fig. 3c &d).** In fact, dCjCas9-KRAB-MeCP2(TRD)/[CMV gRNA1] reduced the level of nLuc expression by about 70%, and dSaCas9-KRAB-MeCP2(TRD)/[CMV gRNA1] lowered it by about 80%. The KRAB-MeCP2 vectors expressing CMV gRNA2 were less potent than those with gRNA1, but still effective: dCjCas9-KRAB-MeCP2(TRD) [CMV gRNA2] suppressed nLuc expression by about 50%, and dSaCas9-KRAB-MeCP2(TRD)/[CMV gRNA2] reduced it by about 60%. Interestingly, gRNA1 consistently outperformed gRNA2, showing greater reductions in luciferase signal across all effectors, not just KRAB-MeCP2(TRD) (**Fig. 3c, d)**. These results are consistent with earlier findings demonstrating that higher levels of repression are often

achieved when gRNAs are designed to target a locus of interest in the vicinity of the transcription start site (TSS) [15], [24]. Indeed, gRNA1 targets a sequence which is proximal to the TSS, whereas gRNA2 targets an upstream part of the promoter (**Fig. 2f).**

In vitro proof-of-concept

Whether epigenetic perturbations caused by episomally-expressed transgenes can be inherited and persist across generations of quickly dividing cells is not fully understood [24], [47]. Here, we aimed to analyze the dynamics of silencing and possible reactivation after an extra-chromosomally expressed CRISPR/Cas repression system is diluted out following cell divisions. To that end, we transduced HEK293T-derived reporter cells with AAV-gRNA1/SaCas9-KRAB-MeCP2(TRD) and extensively passaged them in the culture over the course of three weeks. The samples were collected at day 7, 14 and 21 post transduction, followed by BCA normalization and a Luciferase assay, as above **(Fig. 3e)**. As shown in **Fig. 3e**, transduction of the cells with the AAV- d*Sa*Cas9-KRAB-MeCP2(TRD) vector rapidly gave rise to gene silencing, which stably persisted through cell divisions. Consistently with the data reported in **Fig. 3c** and **d**, the level of nLuc repression was found to be ~80% at day 7; and ~60% and ~50% after two and three weeks, respectively. These data suggest that the CRISPR-induced repression was readily transmitted across multiple cell divisions, resulting in heritable gene silencing. Importantly, the level of viral DNA was under detectable limit at week 2 and 3 post transduction (data not shown).

In vivo proof-of-concept

Studies using *in vivo* models to evaluate the efficiency, specificity, and safety of AAV delivered CRISPR/dCas9 platforms serve as the "gold standard" in the preclinical stages of drug development. To the best of our knowledge, no study thus far has reported successful epigenetic editing in animals using an all-in-one AAV platforms. Here we aimed to validate our lead epigenome editing platform *in vivo*, in the mouse hippocampus. The hippocampus is the primary affected brain region in late onset Alzheimer's disease (LOAD) and related diseases (reviewed in [48]). Therefore we chose this region to assess the potential utility of our platform as a future LOAD therapy.

First, to verify the efficacy of the platform we stereotaxically co-injected the AAV/dSaCas9-KRAB-MeCP2(TRD)/gRNA1 repressor with the LV/dGFP-nLuc reporter (hereafter, LV/GFP) into the left dorsal hippocampus (DH), and co-injected LV/GFP with a no repressor/no gRNA control construct (AAV/dSaCas9) into the right DH, such that each mouse provided an internal control. Six weeks after the injections brains were harvested and GFP expression was compared between the left and right dorsal hippocampus for each mouse. This experiment was performed using a total of 21 C57BL/6 mice, 11 of which (6 males, 5 females) were middle-aged (16 weeks) and the remaining 10 (5 males, 5 females) were very old (32 weeks old). There was no significant difference in GFP expression between males and females, so the data was combined for subsequent analysis. Injection of the AAV/dSaCas9-KRAB-MeCP2(TRD)/gRNA1 vector significantly repressed GFP expression in the left DH compared to the control right DH, in both the middle-aged and the very old mouse groups (middle age – two-tailed Mann-Whitney $U = 18$, $n = 11$, $P = 0.004$; very old – two-tailed Mann-Whitney $U = 21$, $n = 10$, $P = 0.028$; **Fig. 4a, b**). The expression of GFP in the left DH with the AAV/dSaCas9-MeCP2(TRD)/gRNA1 vector was 51.94% ± 11 in the middle-aged group and 40.98% ± 6 in the very old group relative to the right DH with the control vector (**Fig. 4a, b**). There was no significant difference in the efficacy of the repressor between the two age groups. Collectively, the AAV/dSaCas9-MeCP2(TRD)/gRNA1 repressor effectively reduced GFP reporter expression by ~50-60% in mouse dorsal hippocampus.

APOE is the strongest and most reproducible genetic risk factor for LOAD, and an emerging therapeutic target for the disease (reviewed in [49]). Thus, we next investigated the *in vivo* efficacy of our all-in-one AAV epigenome-editing platform using *APOE* as a therapeutically relevant target. As above,

we chose the dorsal hippocampus as a LOAD-relevant brain region. Note however that this experiment aimed to suppress endogenous ApoE expression, as opposed to an artificially-expressed reporter. Two all-in-one AAV repressor vectors were used, which carried dSaCas9-KRAB-MeCP2 along with two gRNAs targeting the *APOE* promoter. A total of sixteen mice (8 males, 8 females) received bilateral stereotaxic injection with the AAV/dSaCas9-KRAB-MeCP2(TRD)/[APOEpro gRNA] repressor vector carrying either gRNA1 (n=8) or gRNA2 (n=8) into the right DH, and the AAV/dSaCas9 control vector (no gRNA, no repressor) into the left DH. At six weeks post-injection, the expression of mouse ApoE was quantified via immunohistochemistry and the levels in right DH and left DH were compared for each mouse. Again there was no significant difference in expression between males and females, and the data was combined for subsequent analysis. The results showed that both AAV/dSaCas9-KRAB-MeCP2(TRD)/[APOEpro gRNA] vectors significantly repressed endogenous mouse ApoE expression in the right DH compared to the left DH (gRNA1 – two-tailed Mann-Whitney U = 0, n = 8, P = 0.0002; gRNA2 – two-tailed Mann-Whitney U = 3, n = 8, P = 0.0011; **Fig. 4d, e**). The relative expression of ApoE (right DH/left DH) with gRNA1 and gRNA2 was 28.8% ± 7.07 and 47.16% ± 8.5, respectively (**Fig. 4d, e**). However, there was no significant difference in the efficacy between the two gRNAs (Unpaired t-test, p=0.14). In conclusion, the endogenous expression of mouse ApoE was reduced by ~71% and ~53% by our all-in-one repressor platform carrying gRNA1 and gRNA2, respectively. These results indicate that our epigenomic therapy platform can effectively suppress ApoE expression, and thus bears translational potential towards the development of therapeutics approach to treat, prevent, and/or delay the progression of LOAD.

Finally, we conducted pilot safety evaluations on the *in vivo* experiment subjects by taking daily weights and monitoring welfare criterions. In the GFP reporter experiment, while both age and sex had a significant influence on mouse weight (middle-aged – Male = 26.09 ± 0.06, Female = 22.37 ± 0.1, F(1,10) = 28.97, p = 0.0003; very old – Male = 32.17 ± 0.09, Female = 25.43 ± 0.05, F(1,10) = 37.48, p = 0.0001; two-way ANOVAs), all mice weights were stably maintained during the 42 days between viral vector injection and sacrifice (**Fig. 4c**). Similarly, in the endogenous *APOE* experiments we observed no changes in the weights of the mice during the 42 days following vector injection (**Fig. 4f**). In addition, the mice displayed normal grooming and eating/drinking behaviors. Overall, these analyses did not reveal any safety issues after the stereotaxic injection of our all-in-one AAV platform for gene repression mediated by epigenome editing.

Discussion

In this study we developed a novel all-in-one AAV9/dSaCas9-KRAB-MeCP2(TRD) repressor system for efficient epigenome editing *in vitro* and *in vivo*. We applied the platform in HEK293T reporter cells and demonstrated that a gRNA targeting the core (TSS-proximal) part of the CMV promoter resulted in an approximately 80% reduction in reporter expression. This data was further corroborated by *in vivo* experiments, in which we observed a ~50-60% reduction in the expression of an exogenous GFP reporter and a ~50-70% reduction in the expression of endogenous mouse ApoE following stereotaxic injection of AAV9/dSaCas9-KRAB-MeCP2(TRD) into the mouse hippocampus. The system is based on a backbone-optimized AAV which harbors binding sites for the activating transcription factors Sp1 and NF-kB. We recently utilized a similar approach to improve CRISPR/Cas9 delivery from integrase-deficient and integrase-competent lentiviral vectors [22], [50]. To the best of our knowledge this platform is the first system to deliver all the necessary components for epigenetic editing in a single AAV.

We applied a screening strategy using a lentiviral dual reporter system, and identified dSaCas9-KRAB-MeCP2(TRD) as being the most potent and sustainable Cas9-effector combination for epigenome-mediated repression. Our results support a recent study by Yeo and colleagues, who engineered a highly effective dCas9-KRAB-MeCP2 transcriptional repressor [32]. Nevertheless, their final vector design contained the complete MeCP2 ORF and the bulky SpCas9, and would be vastly oversized for packaging into AAV particles. Most recently, a similar expression cassette was re-cloned into a lentiviral backbone, yielding lenti_dCas9-KRAB-MeCP2 (Andrea Califano, unpublished data; Addgene plasmid #122205). This vector also carried the complete MeCP2 cDNA and with dSpCas9. Here, we report the development of a miniature repressor system using only the MeCP2 transcriptional repression domain (TRD) [51], [52], [53], [54], [43]. The TRD identified in the above studies was sufficient to mediate robust, sustained gene silencing by providing a binding platform for HDAC1/2 and other transcriptional repressors. The TRD that was used in this study comprised amino acid residues 207-310 of MeCP2. The coding sequence of the dSaCas9-KRAB-MeCP2(TRD) transgene was only 3.6 kb long, and the overall size of the vector including promoter, transgene, polyA signal, U6-gRNA cassette, and ITRs was 4.7 kb. With this vector we achieved physical titers of slightly over 10^{13}vg/mL, which is a sufficient titer for most therapeutic applications in humans. Most importantly, the vector demonstrated a high level of gene repression when transduced into cultured cells or mouse hippocampus.

The efficiency and specificity of the epigenome-editing approach has shown great promise for a wide range of gene therapy applications. Initial successes were been reported in many studies, and have inspired efforts to improve and optimize CRISPR/dCas systems for targeting and manipulating DNA at the epigenetic level (reviewed in [24]). These systems bear significant advantages over conventional CRISPR/Cas editing approaches utilizing active Cas enzymes, including (*i*) higher specificity and on-target editing efficiency, (*ii*) lower off-target effects, and (*iii*) an inability to break – or even nick – DNA at the site of interest, resulting in lower toxicity. Similarly, rates of undesired genomic rearrangements such as deletions, duplications, inversions, and translocations are significantly lower when using dead Cas9-based editing systems [15], [31]. Combining CRISPR/dCas9 targeting components with potent epigenetic repressors in a single AAV delivery vector will greatly facilitate studies of gene regulation and the development of new approaches to address gene dysregulation in various disease states.

Adeno-associated vectors (AAVs) represent a “gold-standard” delivery platform for a range of gene therapy applications [23]. Their high efficiency, capacity to robustly transduce both dividing and non-dividing cells, and the ability to persist in non-integrating/transient forms has elevated AAVs to be the platform of choice for applications in both basic and translational research. However, there is a

challenge: AAVs can only carry relatively small transgenes, whose size does not exceed approximately 4.6kb [21]. Several approaches have been developed to circumvent this bottleneck. First, an *in situ* split intein-based approach has been used in which Cas9 is split in half, delivered via two AAVs, and the full protein is reassembled after transduction [55], [56]. The second approach utilizes a simpler type of dual-vector system, in which different components of the repression machinery are delivered from separate AAVs (dCas/effector from one AAV, gRNA cassette from the other) [55], [57], [29]. Although successes have been reported, these approaches usually demonstrate only moderate efficacy, and require higher viral doses to achieve the desired effects. Furthermore, manufacturing of dual-AAV systems is time- and cost-intensive. These shortcomings served as the impetus for our development of an AAV platform capable of efficiently transferring fully functional CRISPR/dCas repressor complexes to a cell or tissue of interest in a single AAV particle. Our all-in-one vector accomplishes exactly that, circumventing AAV packing limitations for the first time. As such, our platform is attractive and advantageous for both basic and translational sciences as well as clinical applications.

It is not currently clear whether transcriptional changes driven by epigenome editing can be inherited in a stable and permanent manner. On the same note, it is not well understood whether epigenetic modifications introduced by epigenome editors will be 'remembered', and propagated by human cells without constitutive and integrated expression of the epigenetic modifier. In fact, it has been demonstrated that programmable epigenetic tools expressed transiently are tunable and reversible [58]. In contrast, other studies have shown that it is feasible to install a stable transcriptional program that is inherited across cell divisions, without integrated expression of the epigenetic modulators [59], [60]. In particular, Amabile et al. demonstrated heritable silencing by recruitment of DNA methyltransferases and KRAB proteins to the target genes. However, this and other approaches aiming to permanently shut down expression of a target of interest are based on a design utilizing either two or three fusion proteins for each gene, which is experimentally cumbersome, especially for multiplexed gene targeting. Furthermore, the multiplexed repressors used in the above studies consistently cannot be delivered by AAV, being far over the size restrictions. Similarly, a TALE-based fusion of KRAB and the DNMT3A and DNMT3L domains resulted in low efficacy but long-term gene repression [61]. A recent study conducted by Thakore and colleagues also demonstrated a transient gene silencing effect [29]. This study used a dual AAV vector system (carrying dSaCas9-KRAB and targeting gRNA, respectively) for gene silencing of Pcsk9, a regulator of cholesterol levels, in the liver of adult mice. Systemic administration of the dual-vector AAV8 system resulted in significant reductions of serum Pcsk9 and cholesterol levels, however this reduction was not sustained [29]. In contrast with those findings, here we demonstrate that significant repression (~50%) of a reporter gene persists for at least three weeks post-transduction in fast-dividing HEK293T cells. By this time point, the cells had multiplied more than 20,000 times and carried no viral genomes (data not shown), suggesting that transient expression of dSaCas9-KRAB-MeCP2(TRD) can cause robust, sustained gene silencing that is 'remembered', and inherited by cells through multiple cell divisions. As such, the mitotically stable 'hit-and-run' epigenome editing approach developed in this study is extremely appealing for correcting dysfunctions in dividing or non-dividing cells, in both*ex vivo* and *in vivo* settings. Even more broadly, the developed viral system can be adjusted to target a cell or tissue of interest by selecting the desired viral serotypes or outfitting the epigenome modifier with a cell- or tissue-specific promoter. And of course, the CRISPR/Cas system can target any sequence of interest by simply switching the gRNA protospacer sequence. Finally, additional regulation may be achievable by our developed platform via repressor and/or gRNAs multiplexing, adding further advantage.

To demonstrate the therapeutic utility and applicability of the platform, we performed validation experiments in the context of CNS disorders and specifically dementia. The hippocampus was selected as it plays a major role in learning and memory and its atrophy is one of the most consistent features in several age related neurodegenerative diseases (NDDs), including Alzheimer's Disease (AD), Huntington's Disease (HD), Frontal-Temporal Dementia (FTD) and Amyotrophic Lateral Sclerosis (ALS) (reviewed in [48], [49], [62]). We chose to target the Apolipoprotein E (*APOE*) gene as it is the strongest and most reproduceable genetic risk factor for late-onset Alzheimer's disease (LOAD), both for overall risk and age-at-onset (AAO) [63-76]. It thus holds promise as a potential therapeutic target for LOAD and related dementias (reviewed in [49]). Indeed, accumulating evidence suggests that increased overall expression of *APOE* plays an important role in the etiology of LOAD (reviewed in [49, 77]). Therefore, we applied our platform to evaluate its potential for downregulating *APOE* gene expression. We demonstrated that levels of endogenous mouse ApoE expression were reduced up to 70% following stereotaxic injection of the AAV/dSaCas9-KRAB-MeCP2(TRD) platform in the mice DH. In addition, our data supports the safety of the platform *in vivo* upon administration into the mouse brain. These outcomes warrant further preclinical investigations in Alzheimer's disease models. Collectively these results suggest that our innovative platform could serve as a promising foundation for the development of a disease modifying therapy (DMT) to prevent, delay the onset of, and/or halt the progression of LOAD. Moreover, the ability to quickly and easily tailor our platform to target genes associated with other neurodegenerative diseases such as *SNCA* in PD, DLB and MSA, broadens the applications of the platform to a wide range of CNS disorders caused by the dysregulation of any number of genes.

Materials and Methods

Plasmid design and construction

The *Cj*Cas9 was derived from the plasmid pX551-CMV-*Cj*Cas9 (addgene, #107035; gift from Alex Hewitt's lab). The plasmid was amplified using the following primers: 1097AgeI- For, 5'-agctctctggctaactac-3' and 1097BamHI- Rev, 5'-cttttattgGatCcttagctggcctcc-3'. The plasmid pBK694 was previously created in the lab and harbors *Sp*Cas9 in an AAV backbone. The EFS-NC promoter was used to drive expression of *Sp*Cas9 in the above backbone. The plasmid was digested with AgeI- BamHI and cloned with the corresponding fragment containing *Cj*Cas9. The resulting plasmid was named pBK1119. We then created the pBK1120 plasmid by replacing the BsmI- PmlI fragment with its counterpart carrying the H559A mutation in the *Cj*Cas9 ORF. The corresponding fragment was synthesized using GenScript synthesis service. The second mutation, inactivated *Cj*Cas9 D8A was introduced into pBK1120 via digestion and replacement of an AgeI- PflMI fragment created using GenScript synthesis service. The resulting plasmid, pBK1124, carried catalytically inactive CjCas9 (dCas9). Then, we created a CjCas9- U6- promoter-gRNA scaffold using the corresponding fragment synthesized via GenScript synthesis service. Next, we introduced a linker sequence containing DraI- SphI- BlpI 41bps site in frame with the CjCas9 protein. The resulting plasmid, pBK1294a, has been used as a common intermediate for the following cloning of all effector peptides fused with d*Cj*Cas9. The repressor-effectors were cloned into SpeI- BmtI restriction sites of pBK1294. The sequences of the repressors can be found in supplementary figure 1.

To create SaCas9-based constructs, we used pX603-AAV-CMV::NLS-dSaCas9(D10A,N580A)-NLS-3xHA-bGHpA that was obtained from addgene (plasmid #61594; gift from Fang Zhang's laboratory). The amplified fragment of 3202bp harboring dCas9 CDS was cloned into pBK694 as described above. The primers contained AgeI-BamHI sites which were used for cloning, as above. The resulting plasmid was pBK1124. The oligo flanked by NdeI-NotI sites was annealed and cloned to create the pBK1129 plasmid. We then amplified the C-terminus of *Sa*Cas9 and replaced it with the mutated version that carried no stop codon. The following oligo was used 5'-ggatcctcaaataaaagatctttgttttcattagatctgtgtgttggttttttgtgtgcggccggtacc-3' to remove the stop codon at the C-terminus of *Sa*Cas9. This plasmid was named pBK1198. Then, we introduced the adaptor sequence downstream from C-terminus of *Sa*Cas9. The sequence was 5'-GATCCggtggaggaagtggcgggtcagggtcgggtggcACTAGTataGCTAGCggaggtggttcgccaaagaagaaacggaaggtg G-3'. The resulting plasmid is pBK1294b. This plasmid has been used as the intermediate vector for cloning all of the d*Sa*Cas9- repressor fragments. The sequence of the repressors paired with d*Sa*Cas9 can be found in supplementary figure 1. The following gRNA oligos targeting the CMV promoter were selected: *Cj*Cas9-to-CMVp-1 5'-cattgacgcaaatgggcggtag-3' *Cj*Cas9-to-CMVp-2 -5'-attgacgtcaatgggagtttgt-3'. *Sa*Cas9- to-CMVp-1 5'- gcccattgacgcaaatgggc-3'; *Sa*Cas9- to-CMVp-2 5'-gtggatagcggtttgactca-3'.(see, also in Fig. 2f). The following gRNA oligos targeting the ApoE promoter were selected: *Sa*Cas9- to-(Apoe)p-1 (derived from pBK1861) 5'- gaggagggggcgggacagg-3'; *Sa*Cas9- to-(Apoe)p-2 (derived from pBK1863) 5'- gtagctcttccctcccaaggt-3'.

pBK533- pLV-EFS-NC-GFP-P2A-Nluc-WPRE was created previously [22]. The MluI- EcoRI fragment containing EFS-NC-*e*GFP-p2a-nLuc from pBK533 was re-cloned into an AAV backbone. The resulting plasmid was named pBK1083. The pBK1034- lentiviral vector plasmid harboring two Sp1 binding sites was used for the subcloning of 2xSp1-EFS-NC-*e*GFP-p2a-nLuc into the AAV backbone. The resultant plasmid, pBK1084, carries 2xSp1 5-ggatcc**GGGCGGGAC***GTTAACGG***GGGCGGAAC**-3'(marked in bold); separated by the linker sequence (marked in italics). The pBK1035- lentiviral vector plasmid

harboring four Sp1 binding sites has been used for the subcloning of 4xSp1-EFS-NC-*e*GFP-p2a-nLuc into the AAV backbone. The resulting plasmid, pBK1085, carries 4xSp1 5'-ggatcc**GGGCGGGAC***GTTAACGG***GGGCGGAAC****GGGCGGGAC***GTTAACGG****GGGCGGAAC**-3'. The Sp1 sites are marked in bold and red; the linker sequences are marked in italics. The pBK1036-lentiviral vector plasmid harboring two NF-kB binding sites has been used for the subcloning of 2x NF-kB -EFS-NC-*e*GFP-p2a-nLuc into the AAV backbone. The resulting plasmid, pBK1086, carries 2x NF-kB. 5'-ggatcc**GGGGACTTTCC***GTTAACGC***GGGGACTTTCC**-3'. The NF-kB sites are marked in bold; the linker sequence is marked in italics. The pBK1037- lentiviral vector plasmid containing four NF-kB binding sites was used for the subcloning of 4x NF-kB -EFS-NC-*e*GFP-p2a-nLuc into the AAV backbone. The resulting plasmid, pBK1087, carries 4x NF-kB. 5'-ggatcc**GGGGACTTTCC***GTTAACGC***GGGGACTTTCC****GGGGGACTTTCC***GTTAACGC****GGGGACTTTCC**-3'. The NF-kB sites are marked in bold; the linker sequences are marked in italics. The lentiviral vector plasmid pBK1038 harboring 2xSP1 and 2xNF-kB binding sites was used for the subcloning of 2xSp1 and 2xNF-kB-EFS-NC-*e*GFP-p2a-nLuc into the AAV backbone. The resulting plasmid, pBK1088, carries 2xSp1 and 2xNF-kB. 5'-ggatcc**GGGCGGGAC***GTTAACGG***GGGCGGAAC**CGTTAACGGGCGTA**GGGGACTTTCC***GTTAACGC***GGGGACTTTCC**-3. The Sp1 and NF-kB sites are marked in bold; the linker sequences are marked in italics. We derived the EF1a promoter from pBK814- pLenti-EF1a-GFP-p2a-Nanoluc-WPRE. The promoter was cloned into pBK533 to create pLV- EF1a -GFP-P2A-Nluc-WPRE. The resulting vector pBK573 has been recorded. pBK573- lentiviral vector plasmid harbored EF1a-GFP-p2a-Nanoluc-WPRE has been used for the subcloning of EF1a promoter into the AAV backbone. The resulting vector pBK1184 has been recorded. To construct the reporter plasmid used in this study for the screening of the epigenetic repressors, pBK59, an empty LV vector was cloned with BamHI- SalI fragments carryingdestabilized dGFP. dGFP was derived from the Lentiviral-TOP-dGFP-reporter (addgene plasmid #14715; gift from Dr. Tannishtha Reya's laboratory). nLuc was subcloned from pBK533- pLV-EFS-NC-GFP-P2A-Nluc-WPRE as described above. The resulting plasmid, pBK1340, is schematically highlighted in fig.2a.

AAV Vector Production

Plasmids were all packaged into AAV9. AAV vectors were generated using a triple transient transfection protocol in HEK293T (ATCC® CRL3216™) human embryonic kidney cells using polyethyleneimine (PEI). FBriefly, for each virus, media for four 25 mm plates of HEK293T cells at 70–80% confluencyconfluencywaswas first changed into Dulbecco's Modified Eagle Medium (DMEM) (Gibco #: 11965-092) without fetal bovine serum (FBS) (Hyclone #: SH30087.01). One hour after triple transfecting the cells with pHelper (12 ug/plate), pAAV *Rep-Cap* (10 ug/plate), and pAAV ITR-expression (6 ug/plate) plasmids using PEI and DMEM, 10% FBS was added to the media. to a final concentration ofAfter 72 hours, cells were collected, and the cell pellets underwent 4 freeze thaw cycles in -80°C. They were sonicatedthen sonicatedbeforebeing purificationusing two rounds of ultracentrifugation on a cesium chloride (CsCl) gradient. After each centrifugation, fractions containing vector genomes were collected and pooled. The purified vectors were then concentrated using Amicon® Ultra-4 Centrifugal Filter Units (UFC810096). Each virus underwentwas washed three times with PBS at 4°C to remove residual CsCl. The resulting vector, and viral stocks were aliquoted and stored at -80°C. The detailed production canprotocol can be found in [78]. AAV titers were determined by SYBR Green qPCR against a standard curve and primer specific to the U6 promotor of the virus. U6/R1: 5'-

gcctatttcccatgattcctt-3'. U6/L1: 5'-aaaactgcaaactacccaagaa-3'. The annealing temperature for the primers was 60°C.

Cell Culture

The HEK293T/pBK1340 cell line was generated through transduction of HEK293T cells (ATCC® CRL3216™) with pLenti-pBK1340, and selected usingusing puromycin. These cells express dGFP and luciferase (nLuc) downstream of a CMV promoter. The dGFP tag provides visual changes of gene repression whereas the luciferase provides higher spatial resolution identifying protein concentration changes over time. Maintenance cells were grown in DMEM (Gibco), supplemented with 10% fetal bovine serum (Gibco), penicillin/streptomycin 1% (Thermo Fisher Scientific), 2mM L-glutamine, 1% MEM NEAA (Gibco), and 1 mM sodium pyruvate (Gibco). To note: the cells were transduced with the MOI=0.1 to ensure 1 copy/cell following the selection. Before AAV transduction, the cells were seeded at 2.5 x 10^5 cells per 12-well plate and cultured in DMEM with 2% FBS with no supplements.

AAV Transduction

At 50% confluency, the HEK293T/pBK1340 line was transduced with AAV/dCas9-repressor vectors. The following vectors were used: AAV/d*Cj*Cas9-HP1a +/- hinge region (fig.2b); AAV/d*Cj*Cas9-HP1b +/- hinge region (fig.2b); AAV/d*Cj*Cas9-MBD1; AAV/d*Cj*Cas9-MBD2; AAV/d*Cj*Cas9-MBD3; AAV/d*Cj*Cas9-NIPP1; AAV/d*Cj*Cas9-MeCP2(TRD); AAV/d*Cj*Cas9-KRAB; AAV/d*Cj*Cas9-KRAB-MeCP2(TRD); AAV/d*Sa*Cas9-HP1a +/- hinge region (fig.2b); AAV/d*Sa*Cas9-HP1b +/- hinge region (fig.2b); AAV/d*Sa*Cas9-MBD1; AAV/d*Sa*Cas9-MBD2; AAV/d*Sa*Cas9-MBD3; AAV/d*Sa*Cas9-NIPP1; AAV/d*Sa*Cas9-MeCP2(TRD); AAV/d*Sa*Cas9-KRAB; AAV/d*Sa*Cas9-KRAB- MeCP2(TRD). The vectors were used at the MOI=50,000 vg/cell. At 48 hourshours post transduction, the cells reached 100% confluency and were split to 40% confluency. Over the course of 21 days, the cells were passaged and harvested at 70% confluency to prevent epigenetic modifications caused by over confluency.

Luciferase Reporter Assay

Cells from each 12-well plate were first harvested and washed twice with 1xPBS before being resuspended in 200 µL of 1xPBS. 50 µL of the cell and 1xPBS mixture were transferred into a 96-well plate bottom white plate (Costar Cat#3922) and lysis buffer from Nano-Glo Luciferase Assay Kit (Promega Cat#N1120) was added directly to the plates following the manufacturer's protocol. The data was obtained using a microplate spectrophotometer (Bio-Rad, Hercules, CA). Total protein concentration, which was determined by DC Protein Assay Set (Bio-Rad, Hercules, CA), was then used for data normalization.

Genome DNA Extraction and AAV Integration Analysis

Genome DNA was extracted from each cell line every 3 – 4 days after transfection or transduction using DNeasy Blood and Tissue Kit (QIAGEN) per the manufacturer's instructions. qPCR was used to quantify the level of AAV integration by replicating viral genome sequences (U6 primers, listed above were used).

Stereotaxic injections into the mouse hippocampus

Male and female C57BL/6 mice weighing 24–30g were obtained from Charles River Laboratories and investigated at the ages of 16 weeks or 32 weeks. Mice were keptunder standard conditions (21 °C,

12 h/12 h light-dark cycle) with food and water available *ad libitum* in their home cages. All animal protocols were approved by the Duke Institutional Animal Care and Use Committee.

Under isoflurane anesthesia (0.5–2% isoflurane in O2) mice were injected bilaterally into the dorsal hippocampus (DH) via a Neuros syringe (Hamilton) at a rate of 150 nl/minute using the following stereotaxic coordinates (relative to bregma): 1.75 mm anterior, ± 1.5 mm lateral, and 1.55 mm ventral. Mice of 16 weeks and 32 weeks received combination of LV-dGFP-nLuc (LV-GFP) reporter and AAV/gRNA1-d*Sa*Cas9-KRAB-MeCP2(TRD) repressor vector (1 µl) in the left DH, and a combination of LV-GFP reporter and the control vector (no repressor, no gRNA) AAV/d*Sa*Cas (1 µl) in the right DH, providing a within animal control. Mice of 16 weeks received, AAV/gRNA$_{1 \text{ or } 2}$(*Apoe*)p-d*Sa*Cas9-KRAB-MeCP2(TRD) repressor vector (1 µl) in the right DH and the control vector AAV/d*Sa*Cas (1 µl) in the left DH. Animal welfare and weights were monitored daily for 42 days. At 42 days post-injection, mice were transcardially perfused with 10% formalin and coronal slices (100 µm) containing the hippocampus were cut with a vibratome (VT1000S, Leica Microsystems).

Immunohistochemistry

Brain slices were immersed for 1 h at room temperature in PBS containing 0.2% Triton-X 100, 5% normal goat serum and 1x fish gelatin, then incubated with primary antibody for ApoE (1:800, ab183597, Abcam) at 4°C overnight on a rotator. The next day, the slices were rinsed 3 times in PBS and incubated in the corresponding secondary antibody (1:500, Invitrogen, thermo Fisher Scientific) at 4°C overnight on a rotator. Slices were then washed three times with PBS, mounted with VECTASHIELD + DAPI and coverslipped. All slices were imaged under a 2x objective on a fluorescence microscope (Keyence BZ-X810). Images were taken of 3 slices per mouse and analyzed in ImageJ.

Statistical Analysis

For the cell culture experiments, the significance of the differences between no sgRNA and with sgRNA groups were analyzed statistically using student's t test (Realstats Excel). Gene expression was measured via changes in luciferase concentration using a NanoLuc assay. A. A BCA Assay was also conducted to obtain the overall amino acid concentration and to normalize the data. The treated cells were then normalized using the control group of cells transfected/transduced with no sgRNA and no transcriptional repressor domain. Equations (1-2) demonstrate how the luciferase was normalized and quantified.

$$\textit{Percentage of Luciferase (POL)} = \frac{[Luciferase]}{[Total\ Amino\ Acid]} \qquad \textbf{(1)}$$

$$\textit{Normalized Luciferase} = \frac{POL\ in\ Treatment\ Group}{POL\ in\ Control\ Group} \qquad \textbf{(2)}$$

For the mouse experiments, all statistical analysis was performed using GraphPad Prism 9. To determine statistical significance, Shapiro-Wilk tests were first used to evaluate the assumption of normality of the data. For normally distributed data Two-way ANOVA or t-test was used where appropriate, for non-normally distributed data Mann-Whitney test was used.

Funding:
This work was funded in part by the National Institutes of Health/National Institute on Aging (NIH/NIA) [R41 AG077992, R01 AG057522 and RF1 AG077695 to O.C-F.] and the Duke's Viral Vector core fund.

Disclosure:
Drs. Chiba-Falek and Kantor are inventors of intellectual property related to this research and Duke University filed a patent application for the technology developed in this study. CLAIRIgene has an exclusive, worldwide option agreement from Duke for the related patent portfolio for all fields of use. Drs. Kantor and Chiba-Falek are Co-Founders at CLAIRIgene, LLC.

.

References:

1. Jinek, M., et al., *A programmable dual-RNA-guided DNA endonuclease in adaptive bacterial immunity*. Science, 2012. **337**(6096): p. 816-21.
2. Cong, L., et al., *Multiplex genome engineering using CRISPR/Cas systems.* Science, 2013. **339**(6121): p. 819-23.
3. Mali, P., et al., *RNA-guided human genome engineering via Cas9.* Science, 2013. **339**(6121): p. 823-6.
4. Conti, A. and R. Di Micco, *p53 activation: a checkpoint for precision genome editing?* Genome Med, 2018. **10**(1): p. 66.
5. Mandegar, M.A., et al., *CRISPR Interference Efficiently Induces Specific and Reversible Gene Silencing in Human iPSCs.* Cell Stem Cell, 2016. **18**(4): p. 541-53.
6. Tsai, S.Q. and J.K. Joung, *Defining and improving the genome-wide specificities of CRISPR-Cas9 nucleases.* Nat Rev Genet, 2016. **17**(5): p. 300-12.
7. Bikard, D., et al., *Programmable repression and activation of bacterial gene expression using an engineered CRISPR-Cas system.* Nucleic Acids Res, 2013. **41**(15): p. 7429-37.
8. Gilbert, L.A., et al., *CRISPR-mediated modular RNA-guided regulation of transcription in eukaryotes.* Cell, 2013. **154**(2): p. 442-51.
9. Maeder, M.L., et al., *CRISPR RNA-guided activation of endogenous human genes.* Nat Methods, 2013. **10**(10): p. 977-9.
10. Wu, X., et al., *Genome-wide binding of the CRISPR endonuclease Cas9 in mammalian cells.* Nat Biotechnol, 2014. **32**(7): p. 670-6.
11. Qi, L.S., et al., *Repurposing CRISPR as an RNA-guided platform for sequence-specific control of gene expression.* Cell, 2013. **152**(5): p. 1173-83.
12. Tanenbaum, M.E., et al., *A protein-tagging system for signal amplification in gene expression and fluorescence imaging.* Cell, 2014. **159**(3): p. 635-46.
13. Larson, M.H., et al., *CRISPR interference (CRISPRi) for sequence-specific control of gene expression.* Nat Protoc, 2013. **8**(11): p. 2180-96.
14. Konermann, S., et al., *Genome-scale transcriptional activation by an engineered CRISPR-Cas9 complex.* Nature, 2015. **517**(7536): p. 583-8.
15. Rittiner, J.E., et al., *Gene-Editing Technologies Paired With Viral Vectors for Translational Research Into Neurodegenerative Diseases.* Front Mol Neurosci, 2020. **13**: p. 148.
16. Vojta, A., et al., *Repurposing the CRISPR-Cas9 system for targeted DNA methylation.* Nucleic Acids Res, 2016. **44**(12): p. 5615-28.
17. Liu, X.S., et al., *Editing DNA Methylation in the Mammalian Genome.* Cell, 2016. **167**(1): p. 233-247 e17.
18. Liu, X.S., et al., *Rescue of Fragile X Syndrome Neurons by DNA Methylation Editing of the FMR1 Gene.* Cell, 2018. **172**(5): p. 979-992 e6.
19. Kantor, B., et al., *Downregulation of SNCA Expression by Targeted Editing of DNA Methylation: A Potential Strategy for Precision Therapy in PD*. Mol Ther, 2018. **26**(11): p. 2638-2649.
20. Chen, V., et al., *The mechanistic role of alpha-synuclein in the nucleus: impaired nuclear function caused by familial Parkinson's disease SNCA mutations.* Hum Mol Genet, 2020. **29**(18): p. 3107-3121.
21. Kantor, B., et al., *Methods for gene transfer to the central nervous system.* Adv Genet, 2014. **87**: p. 125-97.
22. Ortinski, P.I., et al., *Integrase-Deficient Lentiviral Vector as an All-in-One Platform for Highly Efficient CRISPR/Cas9-Mediated Gene Editing.* Mol Ther Methods Clin Dev, 2017. **5**: p. 153-164.
23. Kantor, B., et al., *Clinical applications involving CNS gene transfer.* Adv Genet, 2014. **87**: p. 71-124.

651 24. Rittiner, J., et al., *Therapeutic modulation of gene expression in the disease state: Treatment*
652 *strategies and approaches for the development of next-generation of the epigenetic drugs.* Front
653 Bioeng Biotechnol, 2022. **10**: p. 1035543.
654 25. Ran, F.A., et al., *In vivo genome editing using Staphylococcus aureus Cas9.* Nature, 2015.
655 **520**(7546): p. 186-91.
656 26. Kim, E., et al., *In vivo genome editing with a small Cas9 orthologue derived from Campylobacter*
657 *jejuni.* Nat Commun, 2017. **8**: p. 14500.
658 27. Burstein, D., et al., *New CRISPR-Cas systems from uncultivated microbes.* Nature, 2017.
659 **542**(7640): p. 237-241.
660 28. Xu, X., et al., *Engineered miniature CRISPR-Cas system for mammalian genome regulation and*
661 *editing.* Mol Cell, 2021. **81**(20): p. 4333-4345 e4.
662 29. Thakore, P.I., et al., *RNA-guided transcriptional silencing in vivo with S. aureus CRISPR-Cas9*
663 *repressors.* Nat Commun, 2018. **9**(1): p. 1674.
664 30. Chavez, A., et al., *Comparison of Cas9 activators in multiple species.* Nat Methods, 2016. **13**(7): p.
665 563-567.
666 31. Nakamura, M., et al., *CRISPR technologies for precise epigenome editing.* Nat Cell Biol, 2021.
667 **23**(1): p. 11-22.
668 32. Yeo, N.C., et al., *An enhanced CRISPR repressor for targeted mammalian gene regulation.* Nat
669 Methods, 2018. **15**(8): p. 611-616.
670 33. Duke, C.G., et al., *An Improved CRISPR/dCas9 Interference Tool for Neuronal Gene Suppression.*
671 Front Genome Ed, 2020. **2**: p. 9.
672 34. Kantor, B., et al., *Notable reduction in illegitimate integration mediated by a PPT-deleted,*
673 *nonintegrating lentiviral vector.* Mol Ther, 2011. **19**(3): p. 547-56.
674 35. Poon, A.P., H. Gu, and B. Roizman, *ICP0 and the US3 protein kinase of herpes simplex virus 1*
675 *independently block histone deacetylation to enable gene expression.* Proc Natl Acad Sci U S A,
676 2006. **103**(26): p. 9993-8.
677 36. Nevels, M., C. Paulus, and T. Shenk, *Human cytomegalovirus immediate-early 1 protein*
678 *facilitates viral replication by antagonizing histone deacetylation.* Proc Natl Acad Sci U S A, 2004.
679 **101**(49): p. 17234-9.
680 37. Richart, A.N., et al., *Characterization of chromoshadow domain-mediated binding of*
681 *heterochromatin protein 1alpha (HP1alpha) to histone H3.* J Biol Chem, 2012. **287**(22): p. 18730-
682 7.
683 38. Monahan, P.E., et al., *Proteasome inhibitors enhance gene delivery by AAV virus vectors*
684 *expressing large genomes in hemophilia mouse and dog models: a strategy for broad clinical*
685 *application.* Mol Ther, 2010. **18**(11): p. 1907-16.
686 39. Kantor, B., et al., *Epigenetic activation of unintegrated HIV-1 genomes by gut-associated short*
687 *chain fatty acids and its implications for HIV infection.* Proc Natl Acad Sci U S A, 2009. **106**(44): p.
688 18786-91.
689 40. Pereira, D.J. and N. Muzyczka, *The cellular transcription factor SP1 and an unknown cellular*
690 *protein are required to mediate Rep protein activation of the adeno-associated virus p19*
691 *promoter.* J Virol, 1997. **71**(3): p. 1747-56.
692 41. Van Lint, C., et al., *A transcriptional regulatory element is associated with a nuclease-*
693 *hypersensitive site in the pol gene of human immunodeficiency virus type 1.* J Virol, 1994. **68**(4):
694 p. 2632-48.
695 42. Goffin, V., et al., *Transcription factor binding sites in the pol gene intragenic regulatory region of*
696 *HIV-1 are important for virus infectivity.* Nucleic Acids Res, 2005. **33**(13): p. 4285-310.
697 43. Razin, A. and B. Kantor, *DNA methylation in epigenetic control of gene expression.* Prog Mol
698 Subcell Biol, 2005. **38**: p. 151-67.

699 44. Lee, D.H., et al., *Comparison of three heterochromatin protein 1 homologs in Drosophila.* J Cell
700 Sci, 2019. **132**(3).
701 45. Smothers, J.F. and S. Henikoff, *The hinge and chromo shadow domain impart distinct targeting*
702 *of HP1-like proteins.* Mol Cell Biol, 2001. **21**(7): p. 2555-69.
703 46. Dong, W. and B. Kantor, *Lentiviral Vectors for Delivery of Gene-Editing Systems Based on*
704 *CRISPR/Cas: Current State and Perspectives.* Viruses, 2021. **13**(7).
705 47. Policarpi, C., J. Dabin, and J.A. Hackett, *Epigenetic editing: Dissecting chromatin function in*
706 *context.* Bioessays, 2021. **43**(5): p. e2000316.
707 48. Vercruysse, P., et al., *Hypothalamic Alterations in Neurodegenerative Diseases and Their*
708 *Relation to Abnormal Energy Metabolism.* Front Mol Neurosci, 2018. **11**: p. 2.
709 49. Yang, A., B. Kantor, and O. Chiba-Falek, *APOE: The New Frontier in the Development of a*
710 *Therapeutic Target towards Precision Medicine in Late-Onset Alzheimer's.* Int J Mol Sci, 2021.
711 **22**(3).
712 50. Vijayraghavan, S. and B. Kantor, *A Protocol for the Production of Integrase-deficient Lentiviral*
713 *Vectors for CRISPR/Cas9-mediated Gene Knockout in Dividing Cells.* J Vis Exp, 2017(130).
714 51. Nan, X., et al., *Transcriptional repression by the methyl-CpG-binding protein MeCP2 involves a*
715 *histone deacetylase complex.* Nature, 1998. **393**(6683): p. 386-9.
716 52. Nan, X., F.J. Campoy, and A. Bird, *MeCP2 is a transcriptional repressor with abundant binding*
717 *sites in genomic chromatin.* Cell, 1997. **88**(4): p. 471-81.
718 53. Hendrich, B. and A. Bird, *Identification and characterization of a family of mammalian methyl-*
719 *CpG binding proteins.* Mol Cell Biol, 1998. **18**(11): p. 6538-47.
720 54. Kantor, B., et al., *Expression and localization of components of the histone deacetylases*
721 *multiprotein repressory complexes in the mouse preimplantation embryo.* Gene Expr Patterns,
722 2003. **3**(6): p. 697-702.
723 55. Chew, W.L., et al., *A multifunctional AAV-CRISPR-Cas9 and its host response.* Nat Methods, 2016.
724 **13**(10): p. 868-74.
725 56. Moreno, A.M., et al., *In Situ Gene Therapy via AAV-CRISPR-Cas9-Mediated Targeted Gene*
726 *Regulation.* Mol Ther, 2020. **28**(8): p. 1931.
727 57. Liao, H.K., et al., *In Vivo Target Gene Activation via CRISPR/Cas9-Mediated Trans-epigenetic*
728 *Modulation.* Cell, 2017. **171**(7): p. 1495-1507 e15.
729 58. Jost, M., et al., *Titrating gene expression using libraries of systematically attenuated CRISPR*
730 *guide RNAs.* Nat Biotechnol, 2020. **38**(3): p. 355-364.
731 59. Amabile, A., et al., *Inheritable Silencing of Endogenous Genes by Hit-and-Run Targeted*
732 *Epigenetic Editing.* Cell, 2016. **167**(1): p. 219-232 e14.
733 60. Van, M.V., T. Fujimori, and L. Bintu, *Nanobody-mediated control of gene expression and*
734 *epigenetic memory.* Nat Commun, 2021. **12**(1): p. 537.
735 61. Mlambo, T., et al., *Designer epigenome modifiers enable robust and sustained gene silencing in*
736 *clinically relevant human cells.* Nucleic Acids Res, 2018. **46**(9): p. 4456-4468.
737 62. Babcock, K.R., et al., *Adult Hippocampal Neurogenesis in Aging and Alzheimer's Disease.* Stem
738 Cell Reports, 2021. **16**(4): p. 681-693.
739 63. Li, Y.J., et al., *Identification of novel genes for age-at-onset of Alzheimer's disease by combining*
740 *quantitative and survival trait analyses.* Alzheimers Dement, 2023.
741 64. Coon, K.D., et al., *A high-density whole-genome association study reveals that APOE is the major*
742 *susceptibility gene for sporadic late-onset Alzheimer's disease.* Journal of Clinical Psychiatry,
743 2007. **68**: p. 613-618.
744 65. Grupe, A., et al., *Evidence for novel susceptibility genes for late-onset Alzheimer's disease from a*
745 *genome-wide association study of putative functional variants.* Human Molecular Genetics, 2007.
746 **16**: p. 865-873.

747 66. Ernoult, E., E. Gamelin, and C. Guette, *Improved proteome coverage by using iTRAQ labelling*
748 *and peptide OFFGEL fractionation.* Proteome Sci, 2008. **6**: p. 27.
749 67. Abraham, R., et al., *A genome-wide association study for late-onset Alzheimer's disease using*
750 *DNA pooling.* BMC Medical Genomics, 2008. **1**: p. 44.
751 68. Bertram, L., et al., *Genome-wide association analysis reveals putative Alzheimer's disease*
752 *susceptibility loci in addition to APOE.* American Journal of Human Genetics, 2008. **83**: p. 623-
753 632.
754 69. Beecham, G.W., et al., *Genome-wide association study implicates a chromosome 12 risk locus for*
755 *late-onset Alzheimer disease.* American Journal of Human Genetics, 2009. **84**: p. 35-43.
756 70. Carrasquillo, M.M., et al., *Genetic variation in PCDH11X is associated with susceptibility to late-*
757 *onset Alzheimer's disease.* Nature Genetics, 2009. **41**: p. 192-198.
758 71. Harold, D., et al., *Genome-wide association study identifies variants at CLU and PICALM*
759 *associated with Alzheimer's disease.* Nature Genetics, 2009. **41**: p. 1088-1093.
760 72. Lambert, J.C., et al., *Genome-wide association study identifies variants at CLU and CR1*
761 *associated with Alzheimer's disease.* Nature Genetics, 2009. **41**: p. 1094-1099.
762 73. Potkin, S.G., et al., *Hippocampal atrophy as a quantitative trait in a genome-wide association*
763 *study identifying novel susceptibility genes for Alzheimer's disease.* PLoS One 4, 2009. **4**: p.
764 e6501.
765 74. Heinzen, E.L., et al., *Genome-wide scan of copy number variation in late-onset Alzheimer's*
766 *disease. Journal of Alzheimer's Disease.* Journal of Alzheimer's Disease, 2010. **19**: p. 69-77.
767 75. Seshadri, S., et al., *Genome-wide analysis of genetic loci associated with Alzheimer disease.*
768 JAMA, 2010. **303**: p. 1832-1840.
769 76. Kamboh, M.I., et al., *Genome-wide association analysis of age-of-onset in Alzheimer's disease.*
770 Molecular Psychiatry, 2012. **17**: p. 1340-1346.
771 77. Gottschalk, W.K., et al., *The Role of Upregulated APOE in Alzheimer's Disease Etiology.* J
772 Alzheimers Dis Parkinsonism, 2016. **6**(1).
773 78. Grieger, J.C., V.W. Choi, and R.J. Samulski, *Production and characterization of adeno-associated*
774 *viral vectors.* Nat Protoc, 2006. **1**(3): p. 1412-28.

775

Fig. 1

a

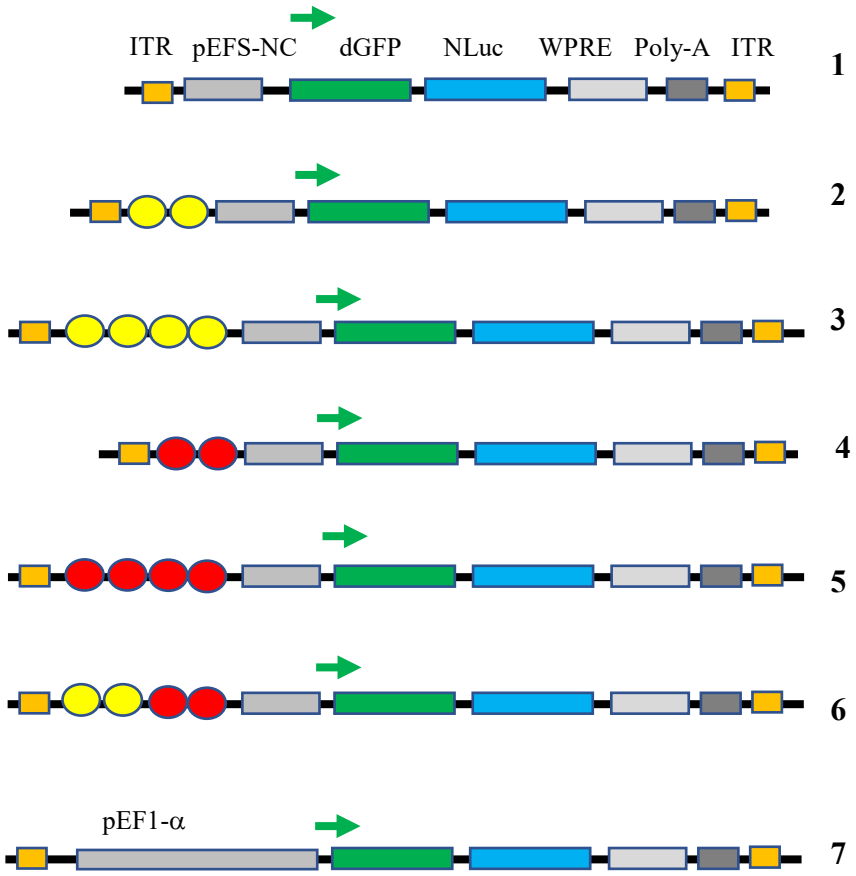
ITR
pEFS-NC
dGFP
NLuc
WPRE
Poly-A
ITR
1
2
3
4
5
6
pEF1-α
7

b

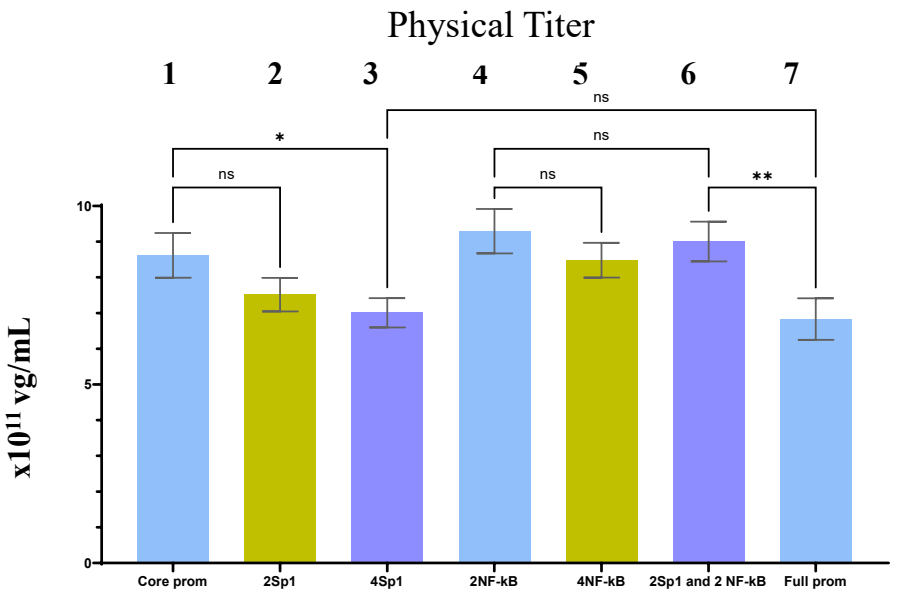
Physical Titer
1
2
3
4
5
6
7
ns
*
ns
ns
ns
**
x10^11 vg/mL
10
5
0
Core prom
2Sp1
4Sp1
2NF-kB
4NF-kB
2Sp1 and 2 NF-kB
Full prom

c

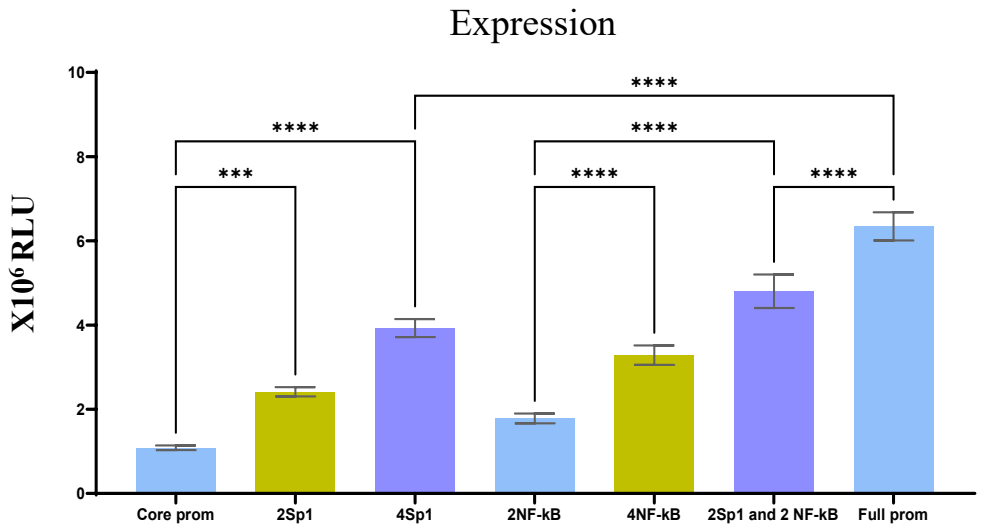
Expression
****
****
***
****
****
****
X10^6 RLU
10
8
6
4
2
0
Core prom
2Sp1
4Sp1
2NF-kB
4NF-kB
2Sp1 and 2 NF-kB
Full prom

Fig. 2

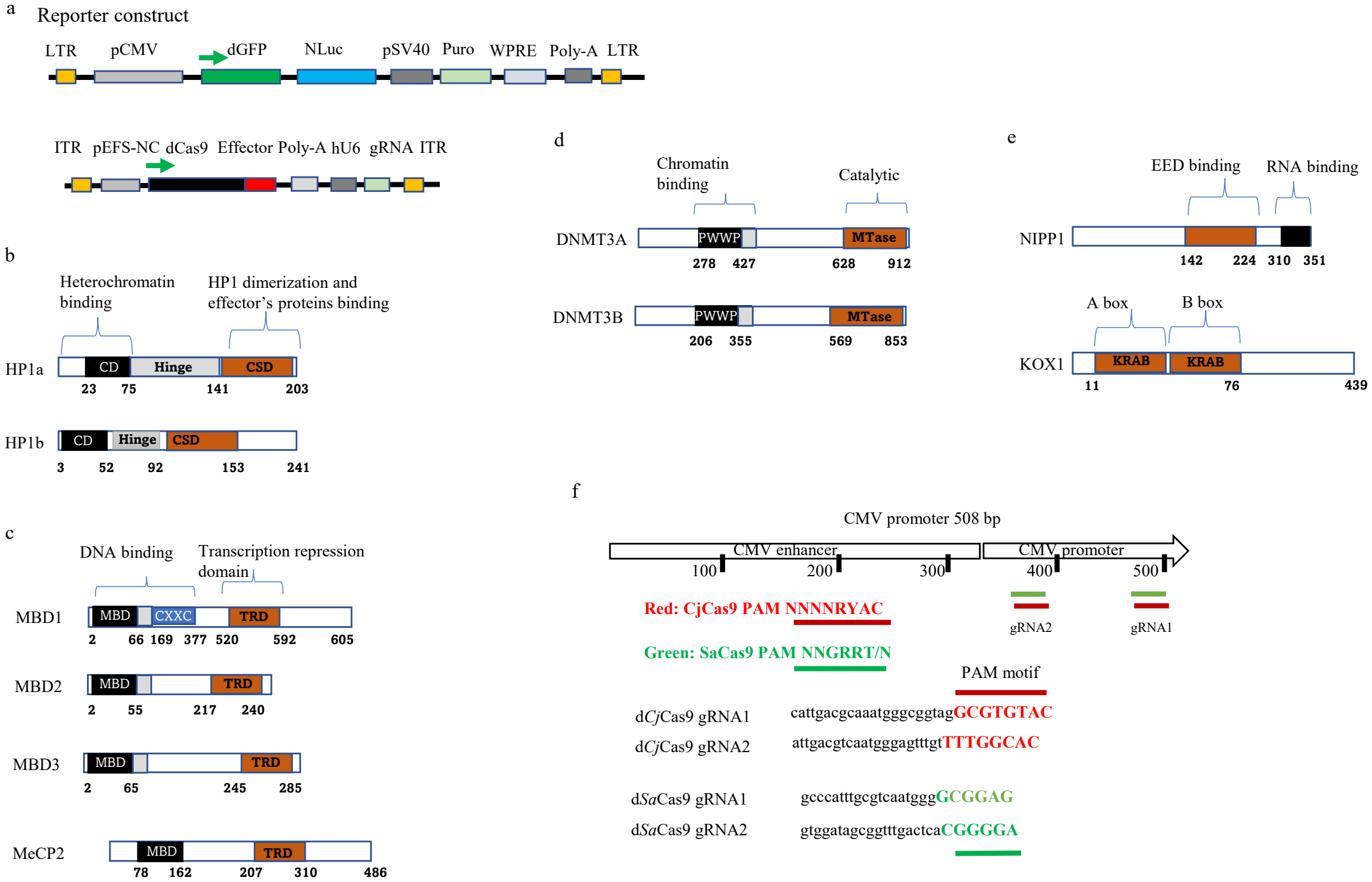
a
Reporter construct
LTR
pCMV
dGFP
NLuc
pSV40
Puro
WPRE
Poly-A
LTR
ITR
pEFS-NC
dCas9
Effector
Poly-A
hU6
gRNA
ITR
b
Heterochromatin binding
HP1 dimerization and effector's proteins binding
HP1a
CD
Hinge
CSD
23
75
141
203
HP1b
CD
Hinge
CSD
3
52
92
153
241
c
DNA binding
Transcription repression domain
MBD1
MBD
CXXC
TRD
2
66
169
377
520
592
605
MBD2
MBD
TRD
2
55
217
240
MBD3
MBD
TRD
2
65
245
285
MeCP2
MBD
TRD
78
162
207
310
486
d
Chromatin binding
Catalytic
DNMT3A
PWWP
MTase
278
427
628
912
DNMT3B
PWWP
MTase
206
355
569
853
e
EED binding
RNA binding
NIPP1
142
224
310
351
A box
B box
KOX1
KRAB
KRAB
11
76
439
f
CMV promoter 508 bp
CMV enhancer
CMV promoter
100
200
300
400
500
Red: CjCas9 PAM NNNNRYAC
gRNA2
gRNA1
Green: SaCas9 PAM NNGRRT/N
PAM motif
dCjCas9 gRNA1
cattgacgcaaatgggcggtagGCGTGTAC
dCjCas9 gRNA2
attgacgtcaatgggagtttgtTTTGGCAC
dSaCas9 gRNA1
gcccatttgcgtcaatgggGCGGAG
dSaCas9 gRNA2
gtggatagcggtttgactcaCGGGGA

Fig. 3

a

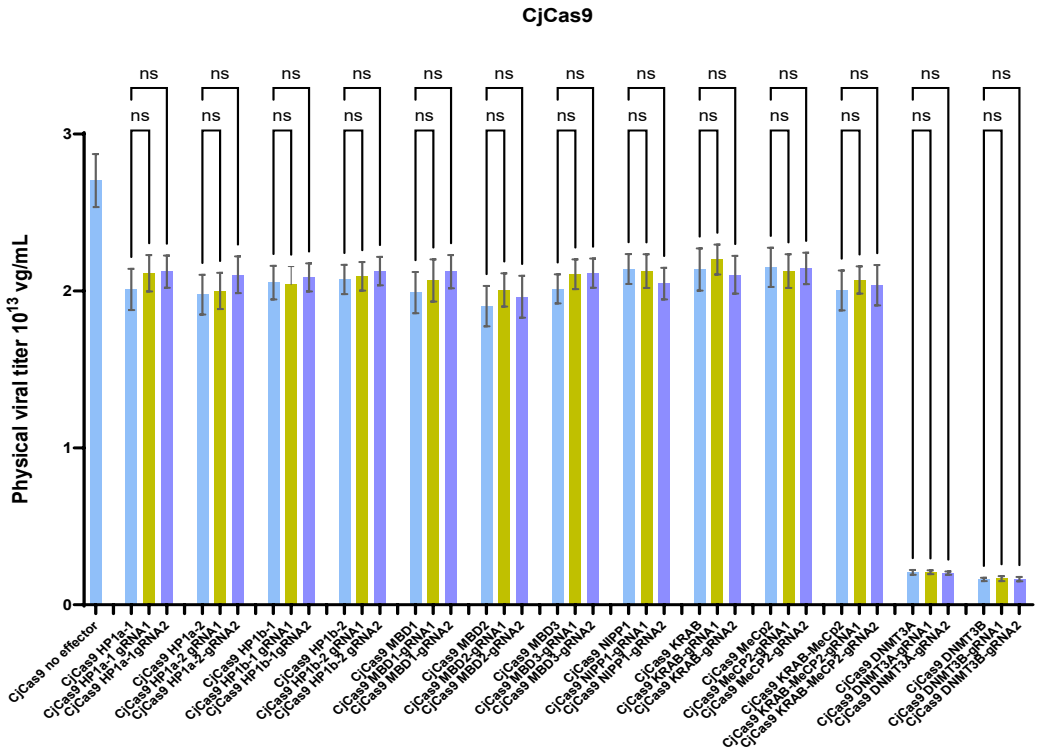
CjCas9
Physical viral titer 10^{13} vg/mL
0
1
2
3
ns
CjCas9 no effector
CjCas9 HP1a-1
CjCas9 HP1a-1 gRNA1
CjCas9 HP1a-1 gRNA2
CjCas9 HP1a-2
CjCas9 HP1a-2 gRNA1
CjCas9 HP1a-2 gRNA2
CjCas9 HP1b-1
CjCas9 HP1b-1 gRNA1
CjCas9 HP1b-1 gRNA2
CjCas9 HP1b-2
CjCas9 HP1b-2 gRNA1
CjCas9 HP1b-2 gRNA2
CjCas9 MBD1
CjCas9 MBD1-gRNA1
CjCas9 MBD1-gRNA2
CjCas9 MBD2
CjCas9 MBD2-gRNA1
CjCas9 MBD2-gRNA2
CjCas9 MBD3
CjCas9 MBD3-gRNA1
CjCas9 MBD3-gRNA2
CjCas9 NIPP1
CjCas9 NIPP1-gRNA1
CjCas9 NIPP1-gRNA2
CjCas9 KRAB
CjCas9 KRAB-gRNA1
CjCas9 KRAB-gRNA2
CjCas9 MeCp2
CjCas9 MeCP2-gRNA1
CjCas9 MeCP2-gRNA2
CjCas9 KRAB-MeCp2
CjCas9 KRAB-MeCP2-gRNA1
CjCas9 KRAB-MeCP2-gRNA2
CjCas9 DNMT3A
CjCas9 DNMT3A-gRNA1
CjCas9 DNMT3A-gRNA2
CjCas9 DNMT3B
CjCas9 DNMT3B-gRNA1
CjCas9 DNMT3B-gRNA2

b

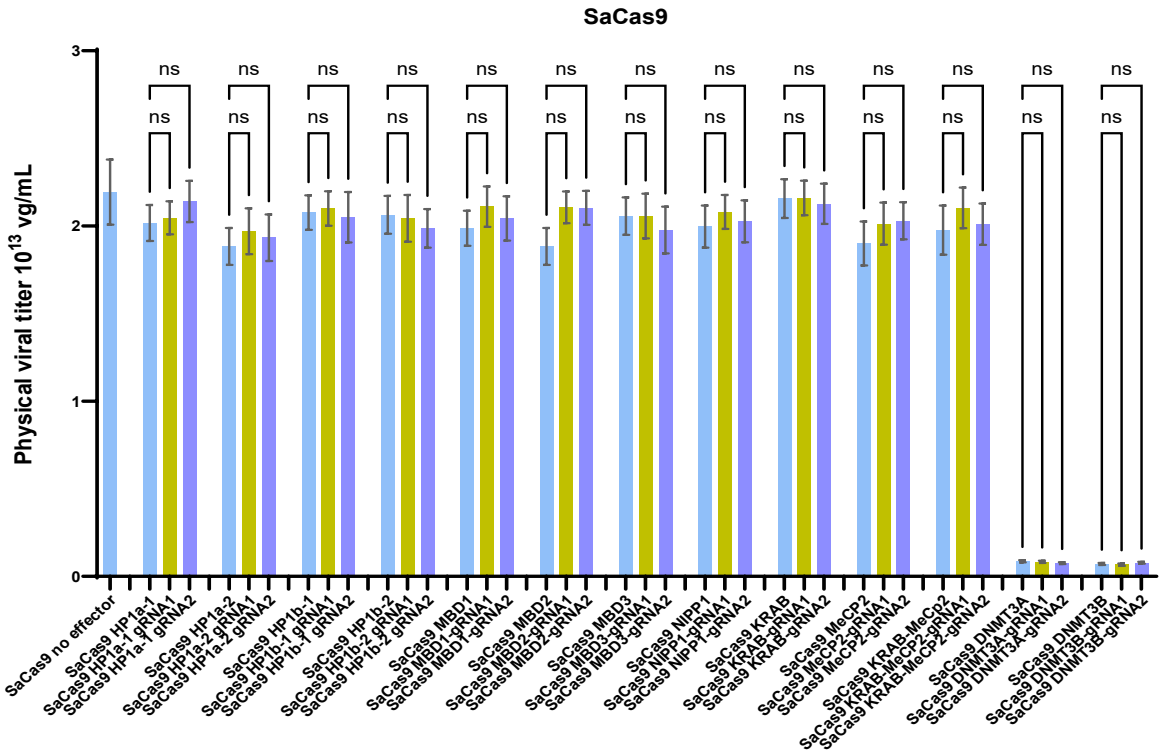
SaCas9
Physical viral titer 10^{13} vg/mL
0
1
2
3
ns
SaCas9 no effector
SaCas9 HP1a-1
SaCas9 HP1a-1 gRNA1
SaCas9 HP1a-1 gRNA2
SaCas9 HP1a-2
SaCas9 HP1a-2 gRNA1
SaCas9 HP1a-2 gRNA2
SaCas9 HP1b-1
SaCas9 HP1b-1 gRNA1
SaCas9 HP1b-1 gRNA2
SaCas9 HP1b-2
SaCas9 HP1b-2 gRNA1
SaCas9 HP1b-2 gRNA2
SaCas9 MBD1
SaCas9 MBD1-gRNA1
SaCas9 MBD1-gRNA2
SaCas9 MBD2
SaCas9 MBD2-gRNA1
SaCas9 MBD2-gRNA2
SaCas9 MBD3
SaCas9 MBD3-gRNA1
SaCas9 MBD3-gRNA2
SaCas9 NIPP1
SaCas9 NIPP1-gRNA1
SaCas9 NIPP1-gRNA2
SaCas9 KRAB
SaCas9 KRAB-gRNA1
SaCas9 KRAB-gRNA2
SaCas9 MeCP2
SaCas9 MeCP2-gRNA1
SaCas9 MeCP2-gRNA2
SaCas9 KRAB-MeCp2
SaCas9 KRAB-MeCP2-gRNA1
SaCas9 KRAB-MeCP2-gRNA2
SaCas9 DNMT3A
SaCas9 DNMT3A-gRNA1
SaCas9 DNMT3A-gRNA2
SaCas9 DNMT3B
SaCas9 DNMT3B-gRNA1
SaCas9 DNMT3B-gRNA2

Fig. 3

c

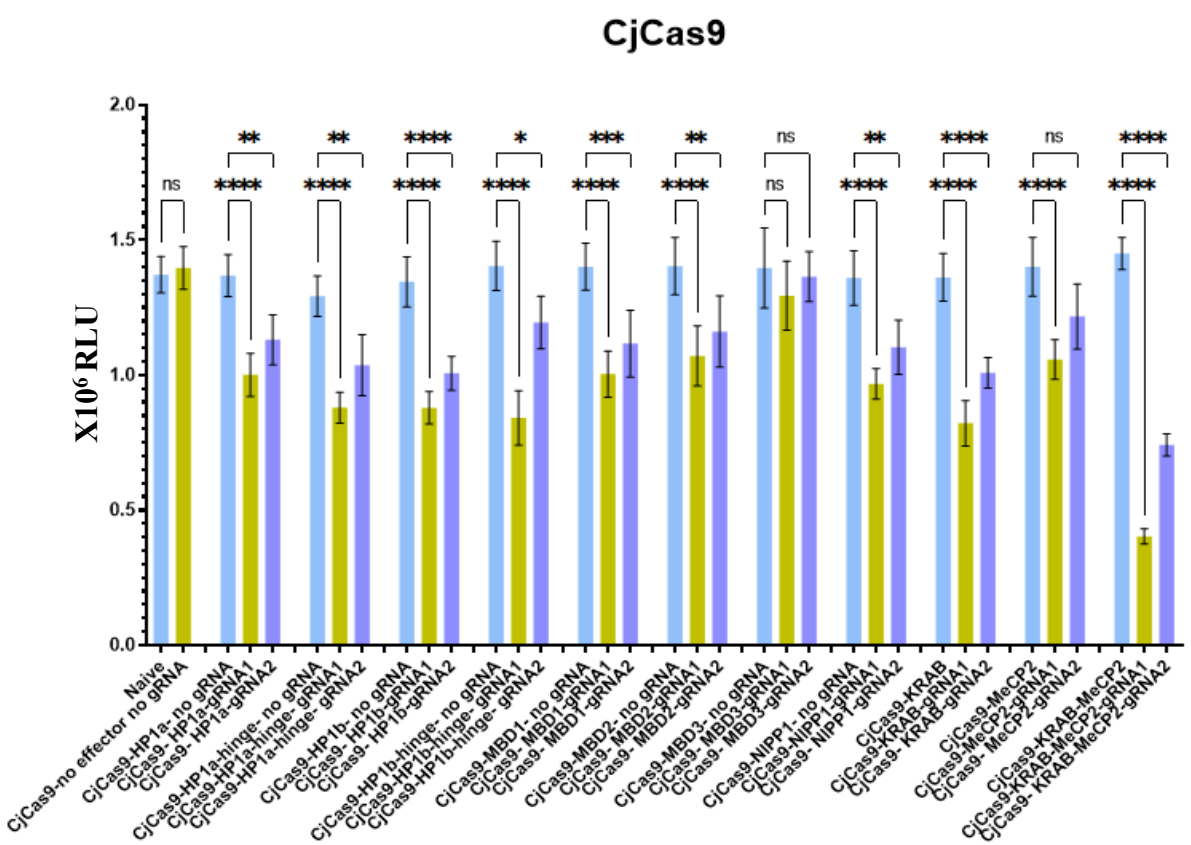
CjCas9
X10⁶ RLU
2.0
1.5
1.0
0.5
0.0
ns
**
****
*
***
Naive
CjCas9-no effector no gRNA
CjCas9-HP1a- no gRNA
CjCas9- HP1a-gRNA1
CjCas9- HP1a-gRNA2
CjCas9-HP1a-hinge- no gRNA
CjCas9-HP1a-hinge- gRNA1
CjCas9-HP1a-hinge- gRNA2
CjCas9-HP1b- no gRNA
CjCas9- HP1b-gRNA1
CjCas9- HP1b-gRNA2
CjCas9-HP1b-hinge- no gRNA
CjCas9-HP1b-hinge- gRNA1
CjCas9-HP1b-hinge- gRNA2
CjCas9-MBD1- no gRNA
CjCas9- MBD1-gRNA1
CjCas9- MBD1-gRNA2
CjCas9-MBD2- no gRNA
CjCas9- MBD2-gRNA1
CjCas9- MBD2-gRNA2
CjCas9-MBD3- no gRNA
CjCas9- MBD3-gRNA1
CjCas9- MBD3-gRNA2
CjCas9-NIPP1- no gRNA
CjCas9-NIPP1-gRNA1
CjCas9- NIPP1-gRNA2
CjCas9-KRAB
CjCas9-KRAB-gRNA1
CjCas9- KRAB-gRNA2
CjCas9-MeCP2
CjCas9-MeCP2-gRNA1
CjCas9- MeCP2-gRNA2
CjCas9-KRAB-MeCP2
CjCas9-KRAB-MeCP2-gRNA1
CjCas9- KRAB-MeCP2-gRNA2

d

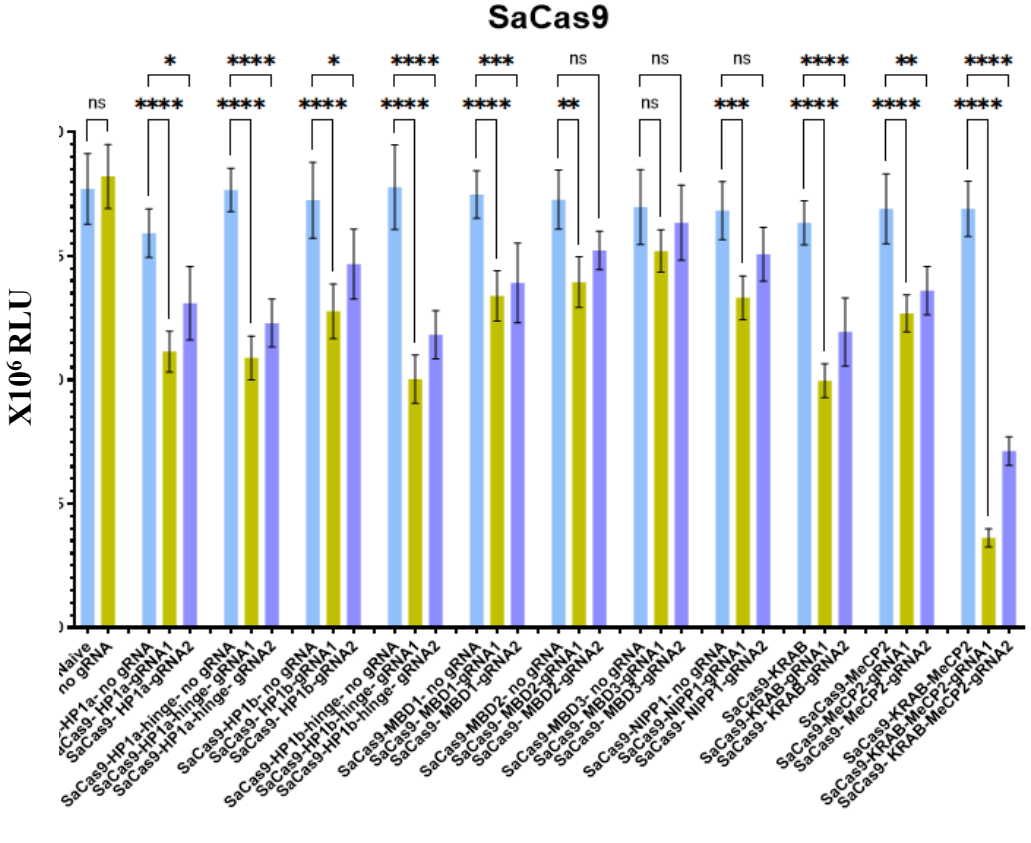
SaCas9
X10⁶ RLU
ns
*
****
***
**
Naive
SaCas9-no gRNA
SaCas9-HP1a- no gRNA
SaCas9- HP1a-gRNA1
SaCas9- HP1a-gRNA2
SaCas9-HP1a-hinge- no gRNA
SaCas9-HP1a-hinge- gRNA1
SaCas9-HP1a-hinge- gRNA2
SaCas9-HP1b- no gRNA
SaCas9- HP1b-gRNA1
SaCas9- HP1b-gRNA2
SaCas9-HP1b-hinge- no gRNA
SaCas9-HP1b-hinge- gRNA1
SaCas9-HP1b-hinge- gRNA2
SaCas9-MBD1- no gRNA
SaCas9- MBD1-gRNA1
SaCas9- MBD1-gRNA2
SaCas9-MBD2- no gRNA
SaCas9- MBD2-gRNA1
SaCas9- MBD2-gRNA2
SaCas9-MBD3- no gRNA
SaCas9- MBD3-gRNA1
SaCas9- MBD3-gRNA2
SaCas9-NIPP1- no gRNA
SaCas9-NIPP1-gRNA1
SaCas9- NIPP1-gRNA2
SaCas9-KRAB
SaCas9-KRAB-gRNA1
SaCas9- KRAB-gRNA2
SaCas9-MeCP2
SaCas9-MeCP2-gRNA1
SaCas9- MeCP2-gRNA2
SaCas9-KRAB-MeCP2
SaCas9-KRAB-MeCP2-gRNA1
SaCas9- KRAB-MeCP2-gRNA2

Fig. 3

e

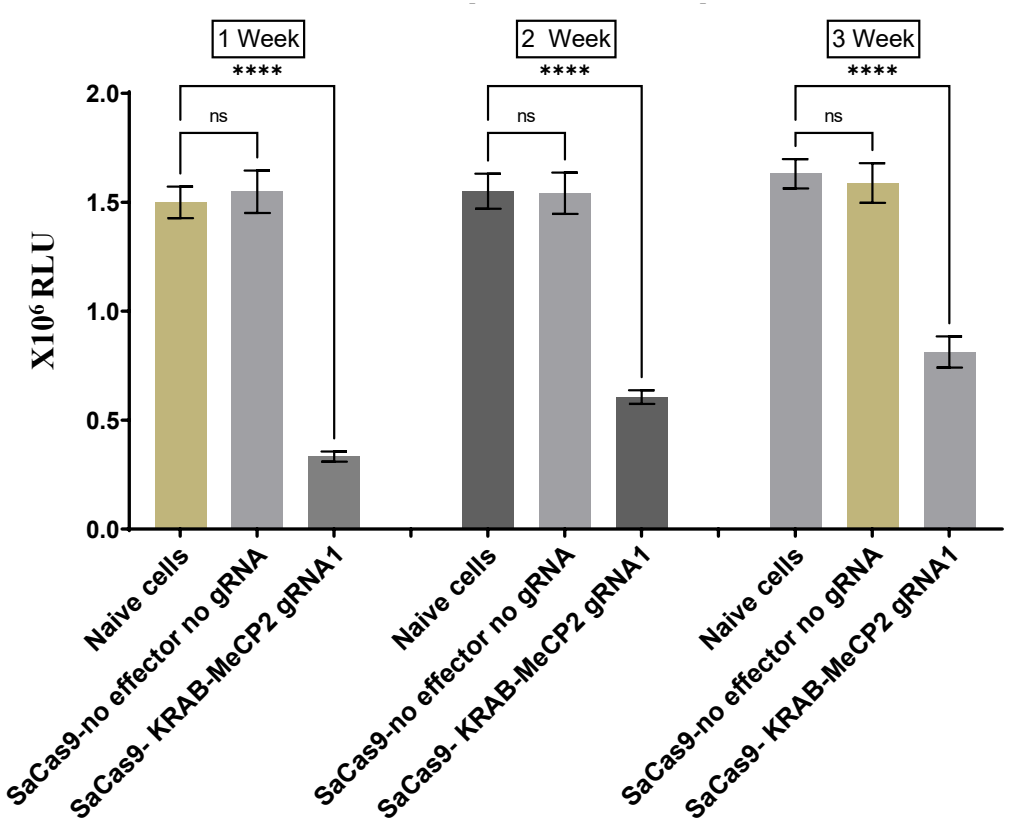
1 Week
2 Week
3 Week
****
ns
X10⁶ RLU
2.0
1.5
1.0
0.5
0.0
Naive cells
SaCas9-no effector no gRNA
SaCas9- KRAB-MeCP2 gRNA1

Fig. 4

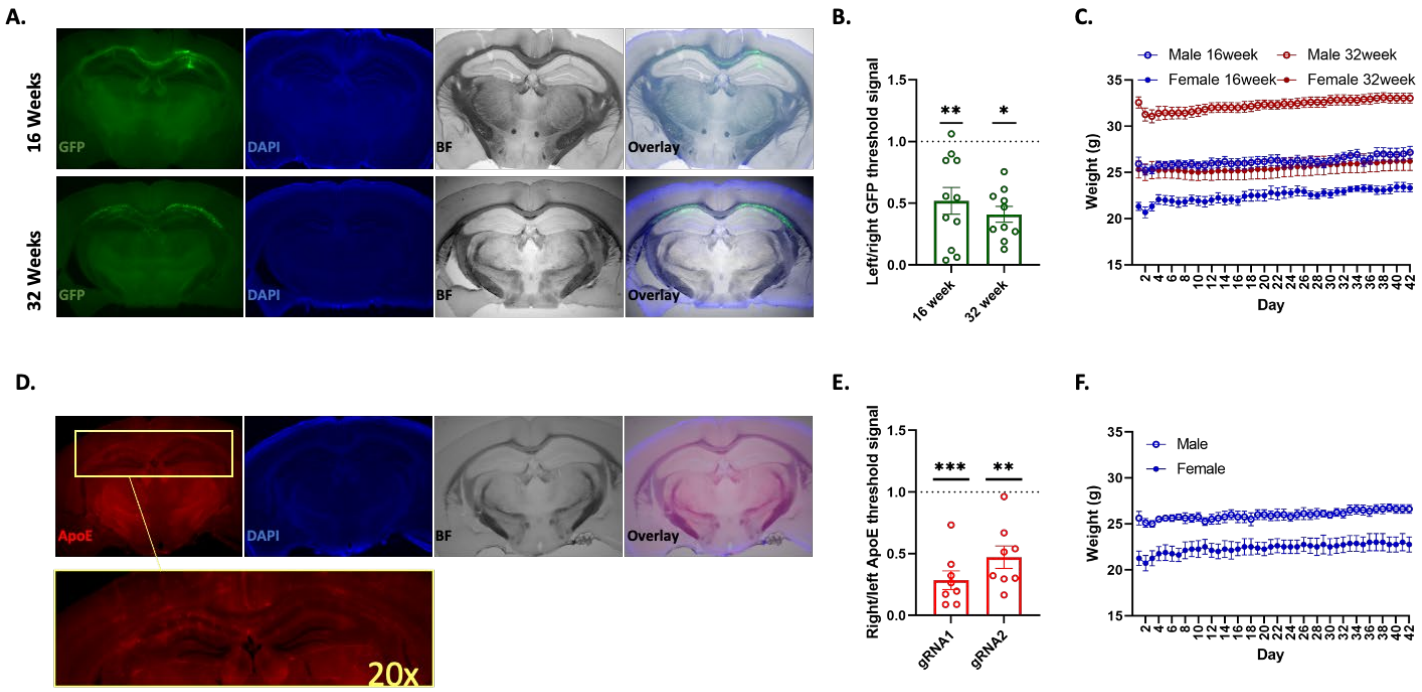
A.
16 Weeks
32 Weeks
GFP
DAPI
BF
Overlay
B.
Left/right GFP threshold signal
16 week
32 week
C.
Male 16week
Male 32week
Female 16week
Female 32week
Weight (g)
Day
D.
ApoE
20x
E.
Right/left ApoE threshold signal
gRNA1
gRNA2
F.
Male
Female

Fig. 1

a

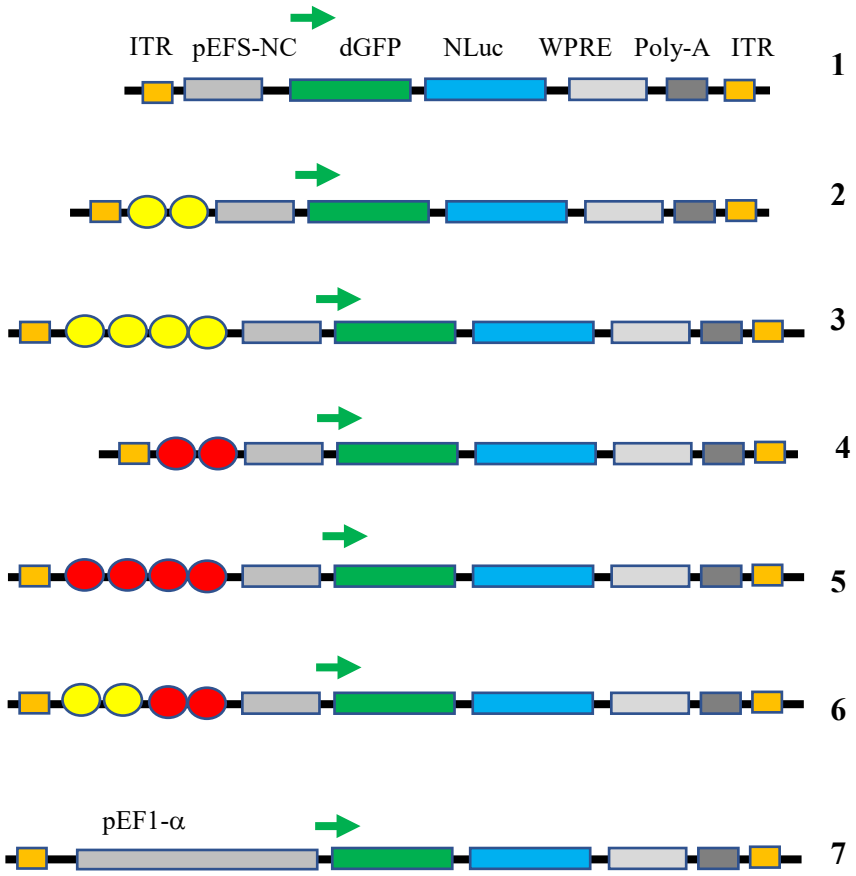
ITR
pEFS-NC
dGFP
NLuc
WPRE
Poly-A
ITR
1
2
3
4
5
6
pEF1-α
7

b

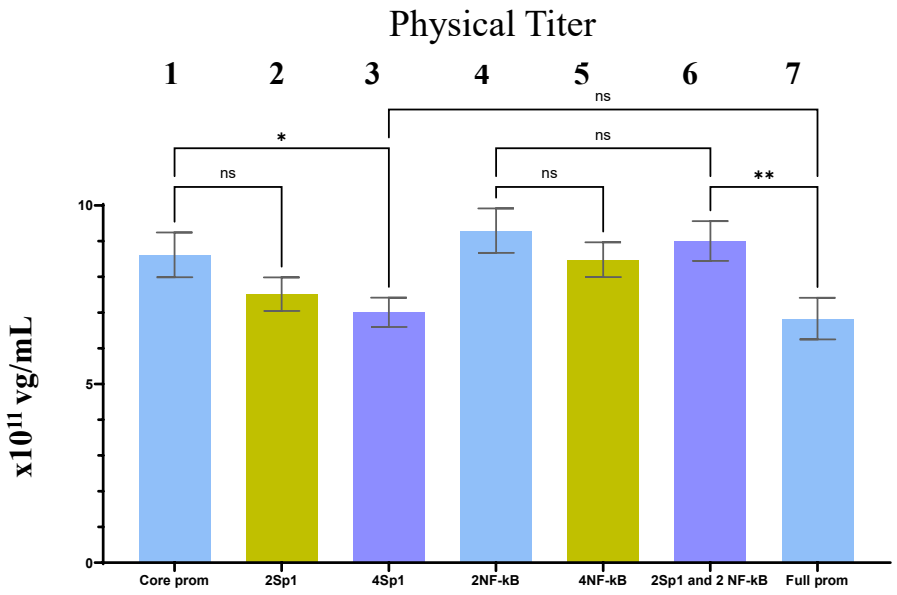
Physical Titer
1
2
3
4
5
6
7
ns
*
ns
ns
ns
**
x10^11 vg/mL
10
5
0
Core prom
2Sp1
4Sp1
2NF-kB
4NF-kB
2Sp1 and 2 NF-kB
Full prom

c

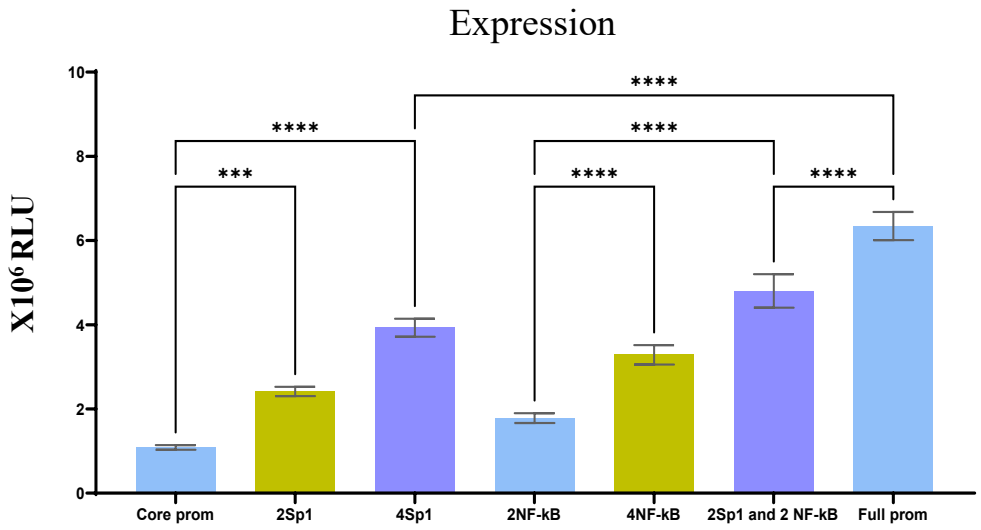
Expression
****
****
***
****
****
****
X10^6 RLU
10
8
6
4
2
0
Core prom
2Sp1
4Sp1
2NF-kB
4NF-kB
2Sp1 and 2 NF-kB
Full prom

Fig. 2

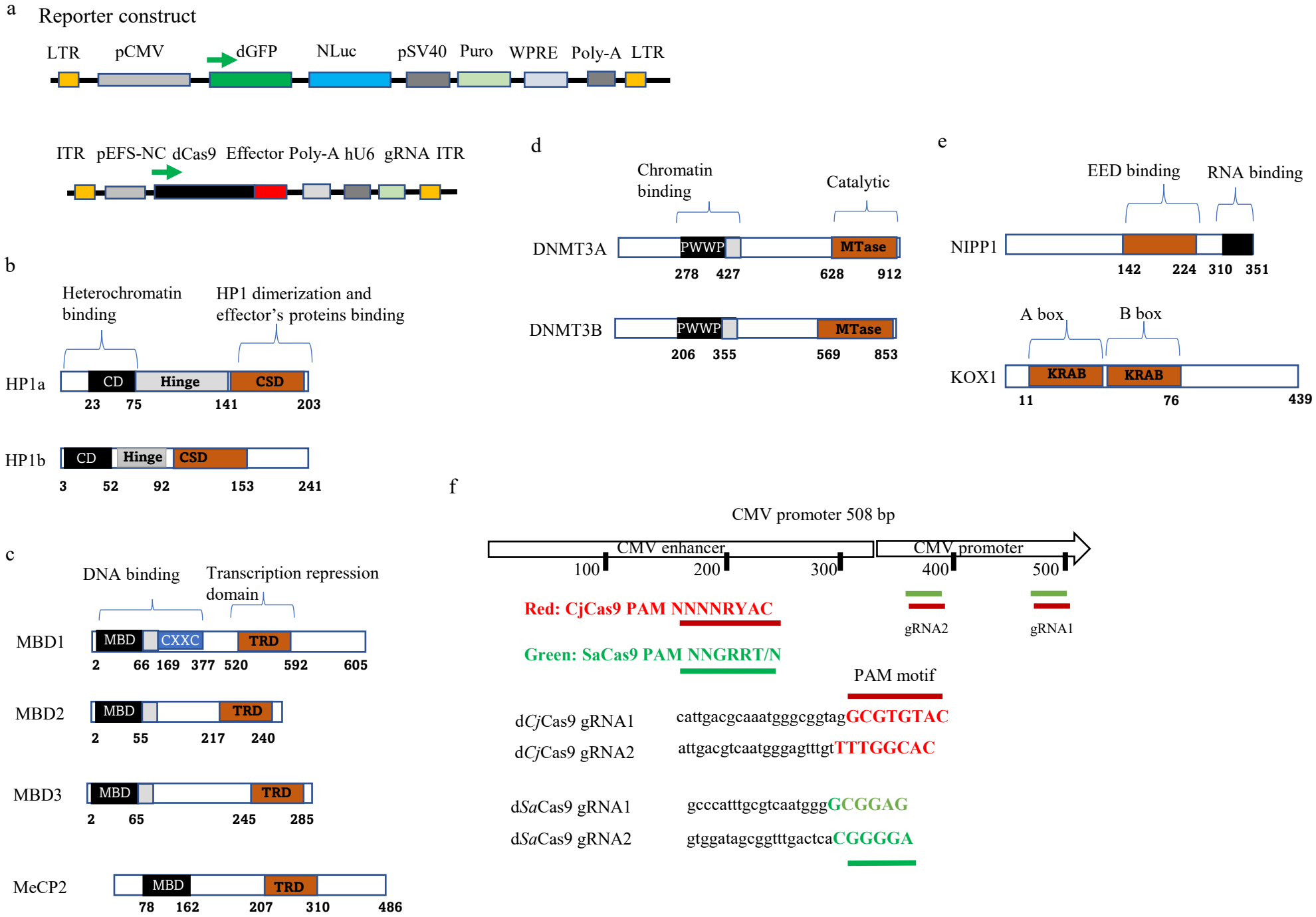
a
Reporter construct
LTR
pCMV
dGFP
NLuc
pSV40
Puro
WPRE
Poly-A
LTR
ITR
pEFS-NC
dCas9
Effector
Poly-A
hU6
gRNA
ITR
b
Heterochromatin binding
HP1 dimerization and effector's proteins binding
HP1a
CD
Hinge
CSD
23
75
141
203
HP1b
CD
Hinge
CSD
3
52
92
153
241
c
DNA binding
Transcription repression domain
MBD1
MBD
CXXC
TRD
2
66
169
377
520
592
605
MBD2
MBD
TRD
2
55
217
240
MBD3
MBD
TRD
2
65
245
285
MeCP2
MBD
TRD
78
162
207
310
486
d
Chromatin binding
Catalytic
DNMT3A
PWWP
MTase
278
427
628
912
DNMT3B
PWWP
MTase
206
355
569
853
e
EED binding
RNA binding
NIPP1
142
224
310
351
A box
B box
KOX1
KRAB
KRAB
11
76
439
f
CMV promoter 508 bp
CMV enhancer
CMV promoter
100
200
300
400
500
gRNA2
gRNA1
Red: CjCas9 PAM NNNNRYAC
Green: SaCas9 PAM NNGRRT/N
PAM motif
dCjCas9 gRNA1
cattgacgcaaatgggcggtagGCGTGTAC
dCjCas9 gRNA2
attgacgtcaatgggagtttgtTTTGGCAC
dSaCas9 gRNA1
gcccatttgcgtcaatgggGCGGAG
dSaCas9 gRNA2
gtggatagcggtttgactcaCGGGGA

Fig. 3

a

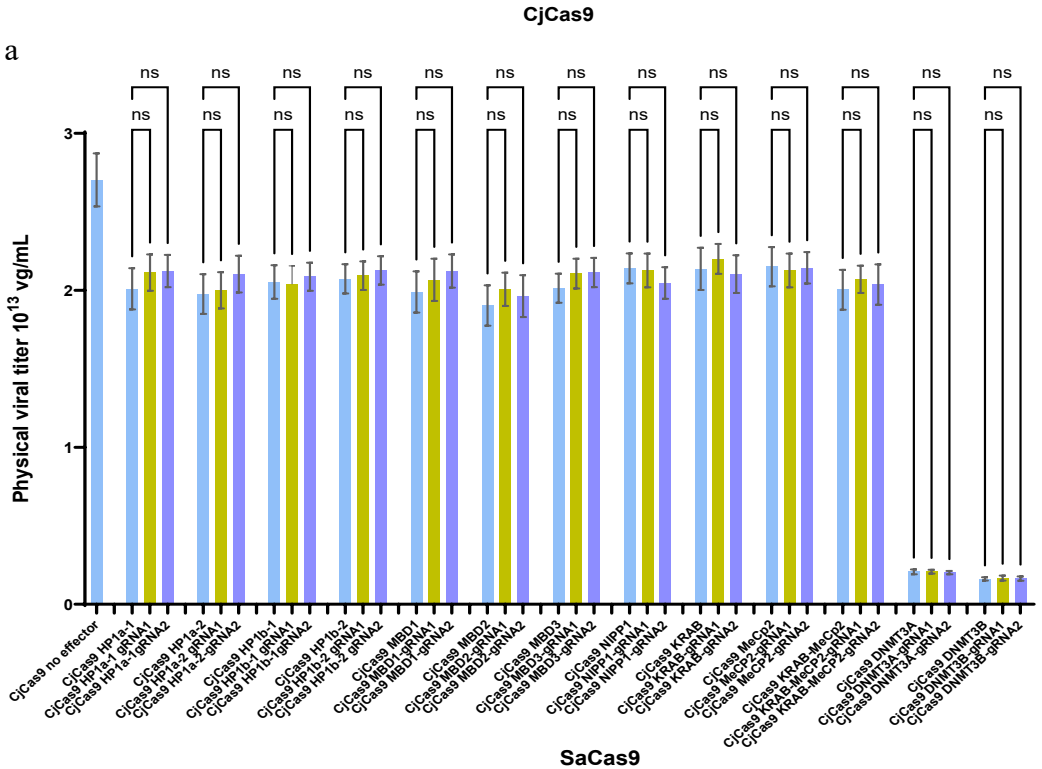
CjCas9
Physical viral titer 10^{13} vg/mL
ns
CjCas9 no effector
CjCas9 HP1a-1
CjCas9 HP1a-1 gRNA1
CjCas9 HP1a-1 gRNA2
CjCas9 HP1a-2
CjCas9 HP1a-2 gRNA1
CjCas9 HP1a-2 gRNA2
CjCas9 HP1b-1
CjCas9 HP1b-1 gRNA1
CjCas9 HP1b-1 gRNA2
CjCas9 HP1b-2
CjCas9 HP1b-2 gRNA1
CjCas9 HP1b-2 gRNA2
CjCas9 MBD1
CjCas9 MBD1-gRNA1
CjCas9 MBD1-gRNA2
CjCas9 MBD2
CjCas9 MBD2-gRNA1
CjCas9 MBD2-gRNA2
CjCas9 MBD3
CjCas9 MBD3-gRNA1
CjCas9 MBD3-gRNA2
CjCas9 NIPP1
CjCas9 NIPP1-gRNA1
CjCas9 NIPP1-gRNA2
CjCas9 KRAB
CjCas9 KRAB-gRNA1
CjCas9 KRAB-gRNA2
CjCas9 MeCP2
CjCas9 MeCP2-gRNA1
CjCas9 MeCP2-gRNA2
CjCas9 KRAB-MeCP2
CjCas9 KRAB-MeCP2-gRNA1
CjCas9 KRAB-MeCP2-gRNA2
CjCas9 DNMT3A
CjCas9 DNMT3A-gRNA1
CjCas9 DNMT3A-gRNA2
CjCas9 DNMT3B
CjCas9 DNMT3B-gRNA1
CjCas9 DNMT3B-gRNA2

b

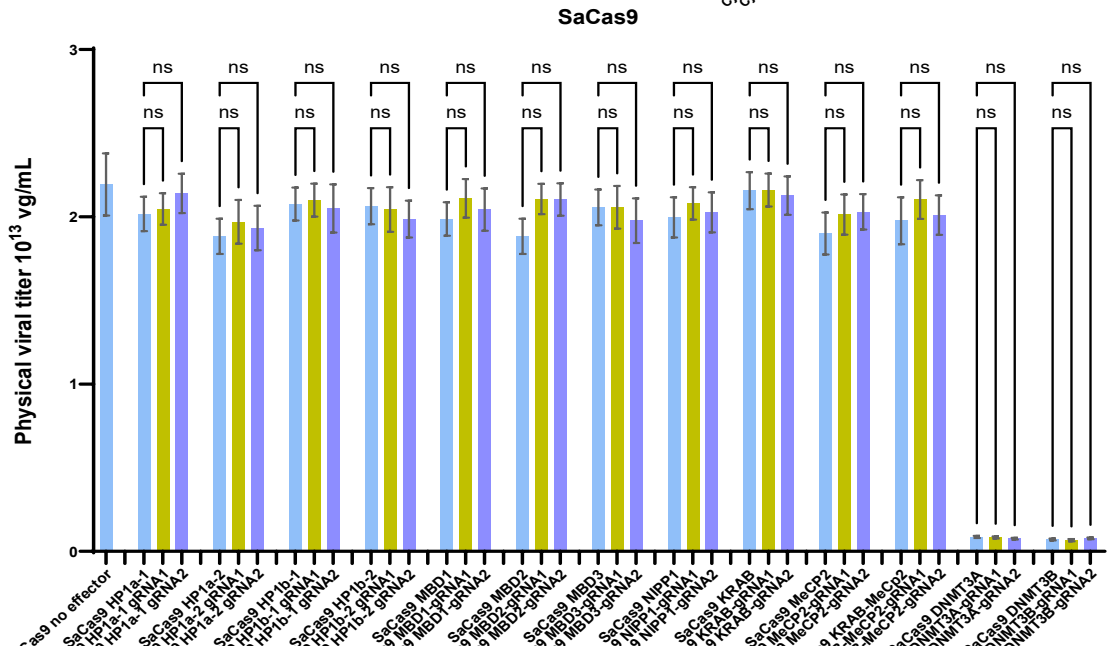
SaCas9
Physical viral titer 10^{13} vg/mL
ns
SaCas9 no effector
SaCas9 HP1a-1
SaCas9 HP1a-1 gRNA1
SaCas9 HP1a-1 gRNA2
SaCas9 HP1a-2
SaCas9 HP1a-2 gRNA1
SaCas9 HP1a-2 gRNA2
SaCas9 HP1b-1
SaCas9 HP1b-1 gRNA1
SaCas9 HP1b-1 gRNA2
SaCas9 HP1b-2
SaCas9 HP1b-2 gRNA1
SaCas9 HP1b-2 gRNA2
SaCas9 MBD1
SaCas9 MBD1-gRNA1
SaCas9 MBD1-gRNA2
SaCas9 MBD2
SaCas9 MBD2-gRNA1
SaCas9 MBD2-gRNA2
SaCas9 MBD3
SaCas9 MBD3-gRNA1
SaCas9 MBD3-gRNA2
SaCas9 NIPP1
SaCas9 NIPP1-gRNA1
SaCas9 NIPP1-gRNA2
SaCas9 KRAB
SaCas9 KRAB-gRNA1
SaCas9 KRAB-gRNA2
SaCas9 MeCP2
SaCas9 MeCP2-gRNA1
SaCas9 MeCP2-gRNA2
SaCas9 KRAB-MeCP2
SaCas9 KRAB-MeCP2-gRNA1
SaCas9 KRAB-MeCP2-gRNA2
SaCas9 DNMT3A
SaCas9 DNMT3A-gRNA1
SaCas9 DNMT3A-gRNA2
SaCas9 DNMT3B
SaCas9 DNMT3B-gRNA1
SaCas9 DNMT3B-gRNA2

Fig. 3

c

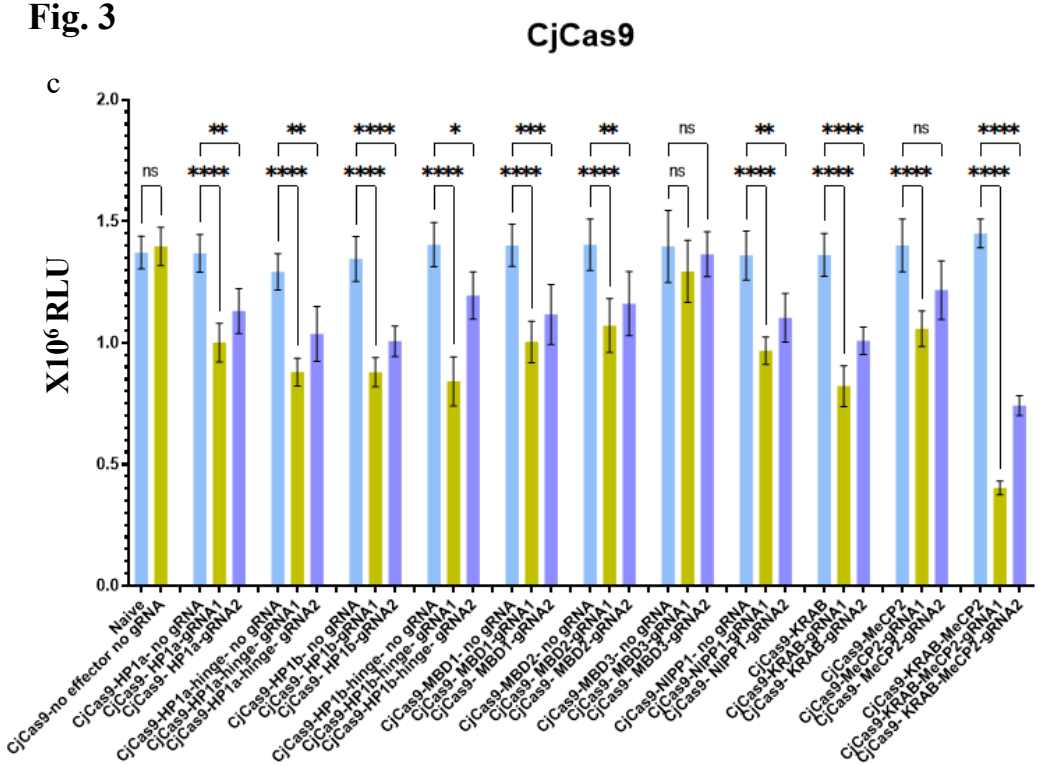
CjCas9
X10⁶ RLU
2.0
1.5
1.0
0.5
0.0
ns
**
****
*
***
Naive
CjCas9-no effector no gRNA
CjCas9-HP1a- no gRNA
CjCas9- HP1a-gRNA1
CjCas9- HP1a-gRNA2
CjCas9-HP1a-hinge- no gRNA
CjCas9-HP1a-hinge- gRNA1
CjCas9-HP1a-hinge- gRNA2
CjCas9-HP1b- no gRNA
CjCas9- HP1b-gRNA1
CjCas9- HP1b-gRNA2
CjCas9-HP1b-hinge- no gRNA
CjCas9-HP1b-hinge- gRNA1
CjCas9-HP1b-hinge- gRNA2
CjCas9-MBD1- no gRNA
CjCas9- MBD1-gRNA1
CjCas9- MBD1-gRNA2
CjCas9-MBD2- no gRNA
CjCas9- MBD2-gRNA1
CjCas9- MBD2-gRNA2
CjCas9-MBD3- no gRNA
CjCas9- MBD3-gRNA1
CjCas9- MBD3-gRNA2
CjCas9-NIPP1- no gRNA
CjCas9- NIPP1-gRNA1
CjCas9- NIPP1-gRNA2
CjCas9-KRAB
CjCas9-KRAB-gRNA1
CjCas9- KRAB-gRNA2
CjCas9-MeCP2
CjCas9-MeCP2-gRNA1
CjCas9- MeCP2-gRNA2
CjCas9-KRAB-MeCP2
CjCas9-KRAB-MeCP2-gRNA1
CjCas9- KRAB-MeCP2-gRNA2

d

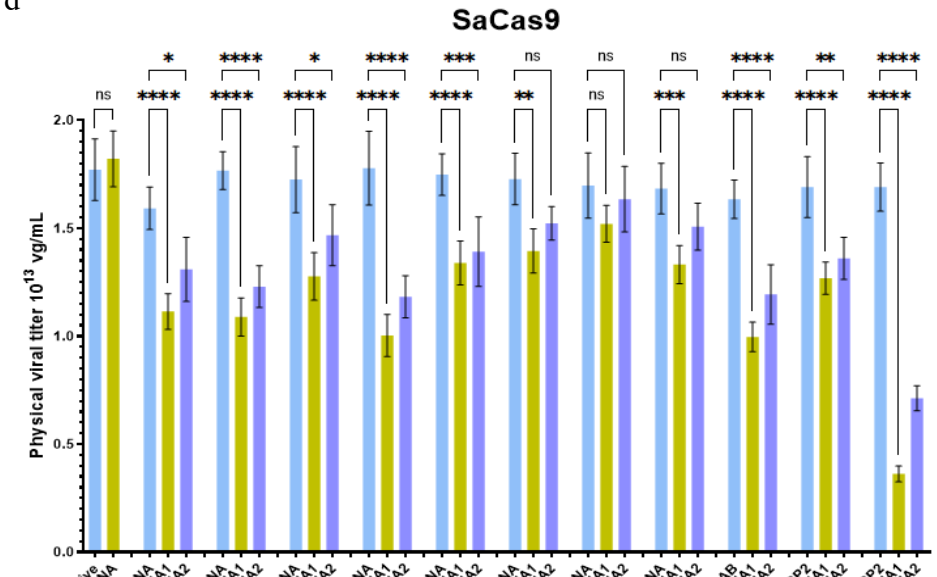
SaCas9
Physical viral titer 10¹³ vg/mL
2.0
1.5
1.0
0.5
0.0
ns
*
**
****
***

Fig. 3

e

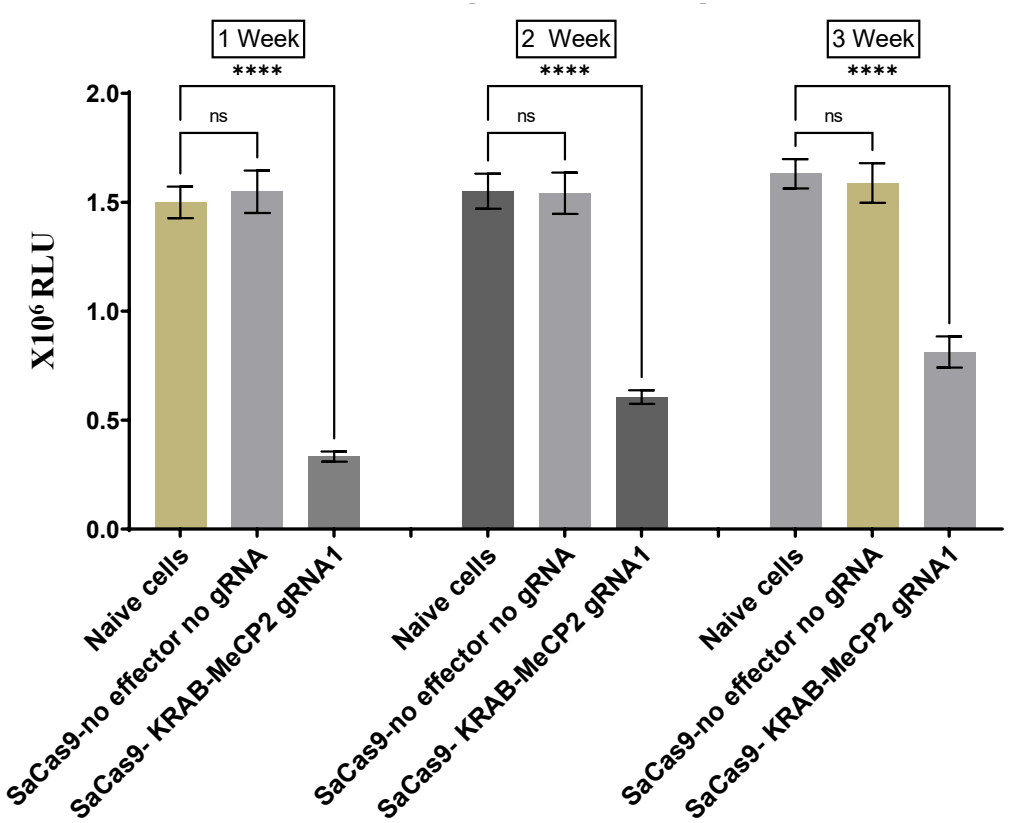
1 Week
2 Week
3 Week
****
ns
X10⁶ RLU
2.0
1.5
1.0
0.5
0.0
Naive cells
SaCas9-no effector no gRNA
SaCas9- KRAB-MeCP2 gRNA1

Fig. 4

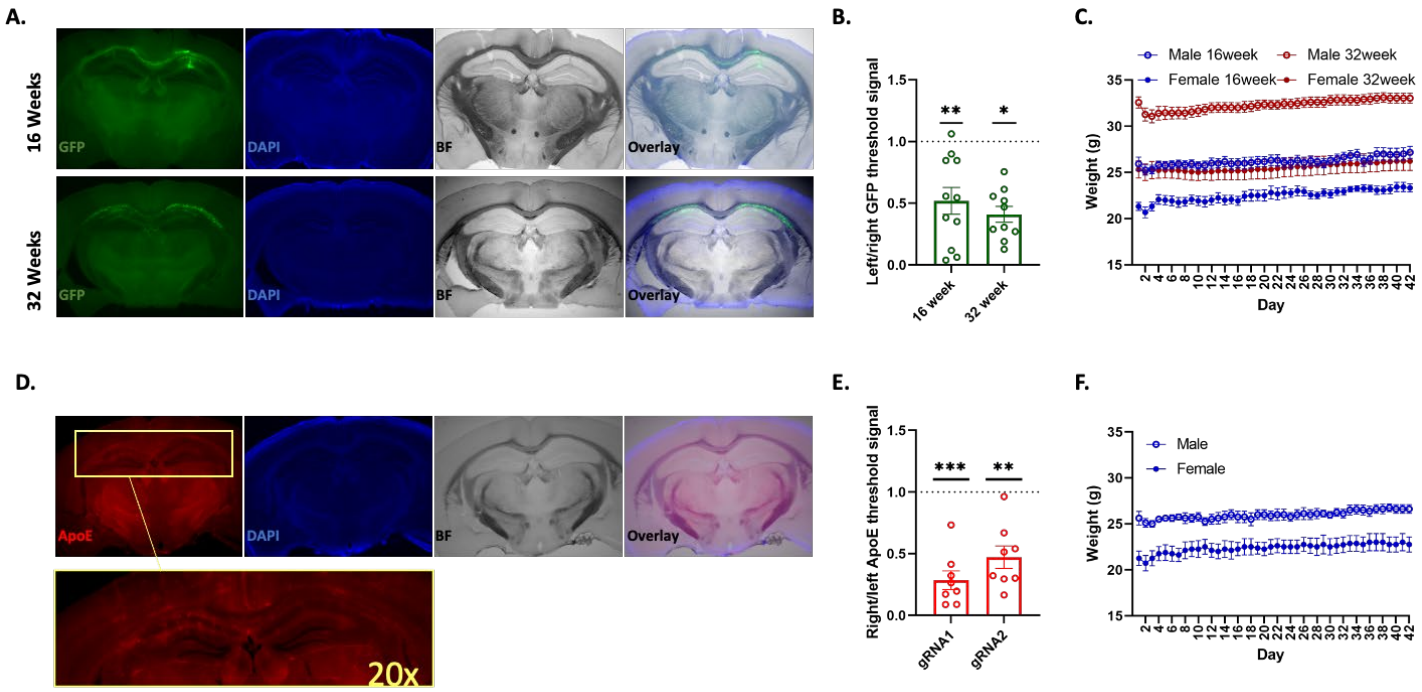
A.
16 Weeks
32 Weeks
GFP
DAPI
BF
Overlay
B.
Left/right GFP threshold signal
16 week
32 week
C.
Male 16week
Male 32week
Female 16week
Female 32week
Weight (g)
Day
D.
ApoE
20x
E.
Right/left ApoE threshold signal
gRNA1
gRNA2
F.
Male
Female

Figure 1: Improvement and optimization of the viral backbone

(a) Sp1 and NF-kB binding sites were introduced upstream from EFS-NC promoter (pEFS-NC) (construct 1). The backbone integrated with 2xSp1 (two yellow circles) is outlined in construct 2. 4xSp1 (four yellow circles) is highlighted in the construct 3. The backbone integrated with 2xNF-kB (two red circles) inserted upstream from pEFS-NC is outlined in the construct 4. The backbone carrying 4xNF-kB (four red circles) is highlighted in the construct 5. 2xSp1/2xNF-kB is depicted in construct 6. The complete EF1a promoter-driven plasmid is outlined in construct 7. The vector carried eGFP – nano-Luciferase reporter. Woodchuck Hepatitis Virus (WHP) Posttranscriptional Regulatory Element (WPRE) is highlighted in the gray box. **(b)** Physical titer of the modified AAV vectors. The titers from the non-concentrated viral preparations were measured by real-time PCR as described in the Materials and Methods. The titers are calculated in vg/mL. The experiment was done in triplicates. The statistical analysis was done using Prism GraphPad software. Ordinary one-way ANOVA was carried out to determine significant difference in the samples' means ± SEM. ns $P > 0.05$, * $P \leq 0.05$, ** $P \leq 0.01$. *** $P \leq 0.001$, **** $P \leq 0.0001$; multiple comparisons of means was determined using Tukey's multiple comparisons test **c)**The expression of the modified AAV vectors has been assessed in HEK293T cells. The Luciferase assay was used to determine Relative Light Units (RLU) signals. In addition, the samples were evaluated on the intensity of the GFP signal via direct visualization using fluorescent scope (data not shown). The experiment was done in quadruplicates. The statistical analysis was done using Prism GraphPad software. Ordinary one-way ANOVA was carried out to determine significant difference in the samples' means ± SEM. ns $P > 0.05$, * $P \leq 0.05$, ** $P \leq 0.01$. *** $P \leq 0.001$, **** $P \leq 0.0001$; multiple comparisons of means was determined using Tukey's multiple comparisons test.

Figure 2: Schematic representation of the screened repressors paired with d*Sa*Cas9 and d*Cj*Cas9

(a) Schematic view of the LV- reporter vector and the parental AAV vector carrying various repressor effectors. LV harbors a dual reporter system consisting of destabilized GFP (dGFP) and nano-Luciferase. Viral long terminal repeats – LTRs; SV40 polyadenylation signal- SV40pA are highlighted.pSV40 drives expression of the puromycin marker. The vector was transduced at the MOI=0.2 to enable selection of the cells carried 1 copy/cell. Woodchuck Hepatitis Virus (WHP) Posttranscriptional Regulatory Element (WPRE). The inverted terminal repeats (ITRs) of AAVare highlighted. The EFS-NC promoter that drives expression of dCas9-effector (black and red boxes, respectively) is highlighted. Human U6 promoter driving expression of gRNA is highlighted. **(b)** Schematic representation of Heterochromatin Protein 1 alpha (HP1a) and Heterochromatin Protein 1 beta (HP1b) The Chromodomain (CD) and Chromoshadow Domain (CSD) are highlighted. The Hinge region separating CD and CSD domains is highlighted**. (c)**Schematic representation of Methyl-Binding Proteins (MBDs):. Methyl-Binding Protein 1 (MBD1); Methyl-Binding Protein 2 (MBD2); Methyl-Binding Protein 3 (MBD3); and Methyl-CpG Binding Protein 2 (MeCP2) are highlighted. Methyl- Binding Domain (MBD) highlighted here, is responsible for the protein-DNA binding Transcription –Repression Domain (TRD) highlighted here is responsible for protein-protein interactions directly involved in gene silencing **d)** Schematic representation of DNA methyltransferases (DNMTs). De novo methyl-transferase A and B (DNMT3A and B, respectively) are highlighted here. The PWWP domain, named for a conserved Pro-Trp-Trp-Pro motif is highlighted. The Methyl-transferase catalytic domains (MTase) of DNMT3A and DNMT3B are highlighted. **e)** Schematic representation of Nuclear inhibitor of Protein phosphatase 1 (NIPP1) protein. Embryonic Ectoderm Development domain (EED) binding to Polycomb Repressive Complex 2 (PRC2) is highlighted. The Krüppel associated box (KRAB) consists of the repressive boxA and boxB domains [1] which is schematically represented. **(f)** Schematic representation of CMV promoter targeted by AAV-KRAB-MeCP2(TRD) system. *Cj*Cas9 –matching gRNA1 and gRNA2 are highlighted. *Sa*Cas9 – matching gRNA1 and gRNA2 are highlighted. PAM of *Cj*Cas9 and *Sa*Cas9 are highlighted.

Figure 3: Titers and expression of the engineered AAV vectors

The titers of the concentrated vectors harboring **(a)** d*Cj*cAS9 and (b)d*Sa*Cas9 were measured using real time PCR. as described in the Material and Methods. The titers are calculated in vg/mL The experiment was done in triplicates. The statistical analysis was done using Prism GraphPad software. Ordinary one-way ANOVA was carried out to determine significant difference in the samples' means ± SEM. ns $P > 0.05$, * $P \leq 0.05$, ** $P \leq 0.01$. *** $P \leq 0.001$, **** $P \leq 0.0001$; multiple comparisons of means was determined using Tukey's multiple comparisons test. Expression of the engineered vectors in the reporter- HEK293T cell line. HEK293T expressing dGFP and nLuc reporters were transduced with AAV vectors harbored different effectors. The vectors carried d*Cj*Cas9 **(c)** and d*Sa*Cas9 **(d)** were titer-normalized prior to the transductions. The samples were harvested 96h post-transduction and the luciferase assay was performed. Relative light units (RLU) were recorded. The experiment was done in quadruplicates. The statistical analysis was done using Prism GraphPad software. Ordinary one-way ANOVA was carried out to determine significant difference in the samples' means ± SEM. ns $P > 0.05$, * $P \leq 0.05$, ** $P \leq 0.01$. *** $P \leq 0.001$, **** $P \leq 0.0001$; multiple comparisons of means was determined using Tukey's multiple comparisons test.**e)** Expression of AAV-d*Sa*Cas9-KRAB-MeCP2(TRD)/gRNA1 in the reporter-HEK293T cell line. The reporter cells were transduced with concentrated and titer=normalized AAV preparations as described above. The samples were harvested 1-, 2- and 3-weeks post-transduction and the luciferase assay was performed. Relative light units (RLU) were recorded. The experiment was done in quadruplicates. The statistical analysis was done using Prism GraphPad software. Ordinary one-way ANOVA was carried out to determine significant difference in the samples' means ± SEM. ns $P > 0.05$, * $P \leq 0.05$, ** $P \leq 0.01$. *** $P \leq 0.001$, **** $P \leq 0.0001$; multiple comparisons of means was determined using Tukey's multiple comparisons test.

Figure 4. *In vivo* validation of the *all-in-one* AAV/ d*Sa*Cas9- KRAB-MeCP2(TRD) repressor platform in mouse hippocampus

The *all-in-one* AAV/ d*Sa*Cas9- KRAB-MeCP2(TRD) repressor platform and the control vector AAV/d*Sa*Cas9 with no repressor were administrated by bilateral stereotaxic injection into the mouse dorsal hippocampus (DH) and validated using a GFP reporter gene (**a-c)** and the mouse endogenous *Apoe* gene (d-f). (**a-b**) The LV-GFP reporter vector was co-injected with the AAV/gRNA1-d*Sa*Cas9- KRAB-MeCP2(TRD) into the left DH and with the control AAV/d*Sa*Cas9 into the right DH. The AAV/gRNA1-d*Sa*Cas9- KRAB-MeCP2(TRD) vector successfully repressed the expression of the GFP reporter gene. (**a**) Representative images of brain coronal slices at 2x magnification 42 days post-injection, showing GFP expression and DAPI staining in the DH. (**b**) The signals were quantified using ImageJ Threshold function. The box plot displays the ratios of the left DH relative to the right DH in both age groups of 16 weeks (n=11) and 32 weeks (n=10) mice. Each open circle represents the quantified signal left/right for a mouse. (**c**) Daily weights post-injection (day 0) through mice were sacrificed (day 42) of 16 weeks (red) and 32 weeks (blue) mice. There was no significant effect on mouse weights. (**d-e**) AAV/gRNA(*Apoe*)p-d*Sa*Cas9-KRAB-MeCP2(TRD) vectors with gRNA 1 or gRNA 2 were injected into the right DH and the control AAV/d*Sa*Cas9 into the left DH. Both AAV/gRNA(*Apoe*)p-d*Sa*Cas9-KRAB-MeCP2(TRD) vectors significantly reduced the mouse endogenous *Apoe* expression. (**d**) Representative images of brain coronal slices at 2x magnification 42 days post-injection, showing *Apoe* expression and DAPI staining in the DH; 20x magnification of DH region showing *Apoe* expression. (**e**) The signals were quantified using ImageJ Threshold function. The box plot displays the ratios of the right DH relative to the left DH for mice injected with the repressor vector harboring gRNA1 (n=8) and gRNA2 (n=8). Each open circle represents the quantified signal right/left for a mouse. (**f**) Daily weights post-injection (day 0) through mice were sacrificed (day 42). There was no significant effect on mouse weights. (16 weeks N=11, 32 weeks N=10, Apoe gRNA1 N=8, Apoe gRNA2 N=8 mice). Values represent mean ± SEM. * $p < 0.05$ ** $p < 0.01$ *** $p < 0.001$; Mann-Whitney U Test.